GEUS Bulletin

RESEARCH ARTICLE

Phosphorus-rich altered basaltic tuff layers with crandallite in Paleocene lake sediments, Nuussuaq Basin, West Greenland

Lotte Melchior Larsen[1]*, Gunver Krarup Pedersen[1], Asger Ken Pedersen[1,2], Nynke Keulen[1], Maja Bar Rasmussen[3], Sebastian Næsby Malkki[1], Henrik Ingermann Petersen[1]

[1]Geological Survey of Denmark and Greenland (GEUS), Copenhagen, Denmark; [2]Natural History Museum of Denmark, Copenhagen, Denmark; [3]Department of Geosciences and Natural Resource Management, Copenhagen University, Copenhagen, Denmark

Abstract

Paleocene mudstones in the Nuussuaq Basin, West Greenland, contain about 20 tuff layers, deposited in the Naajaat–Pingu lakes of the Atanikerluk Formation (*c*. 61 Ma). The tuffs were originally of basaltic composition but are now diagenetically altered, mainly to crandallite, $CaAl_3(PO_4)_2(OH)_5{\cdot}H_2O$, which in most tuffs comprises more than 80% of the rock. All original igneous minerals except chromite are replaced. The tuffs contain up to 18 wt% P_2O_5 and 10 wt% organic carbon. They have high contents of Sr (up to 24 600 ppm), Ba (up to 19 800 ppm) and rare-earth elements (Ce up to 550 ppm) and low contents of SiO_2 (0.4–10 wt%). Nitrogen is identified in some samples. Element enrichment or depletion ratios tuff/basalt are calculated. In total, around 65 wt% of the mass of the original tuff layer, mainly SiO_2, has been replaced by other elements. The least mobile major elements were Al and Ca, which reacted with P to form crandallite. The diagenetic processes in the tuff layers took place soon after deposition and sealing of the layers. The source of phosphorus and carbon, as well as nitrogen, must be organic tissue in which these elements are major components. Only bone material contains sufficient P to form such crandallite-rich layers within a geologically short time. We suggest that volcanic eruptions into the Naajaat–Pingu lakes led to mass mortality, causing fish bones, teeth and scales to accumulate on the lake floor in association with the tuff. The commonly found association of tuff layers with crandallite is a result of two conditions brought together by volcanic eruptions: an abundance of easily degradable volcanic glass and an abundance of organic material rich in phosphorus such as bone.

1 Introduction

Rare occurrences of the hydrated calcium-aluminium-phosphate mineral crandallite, $CaAl_3(PO_4)_2(OH)_5{\cdot}H_2O$ have been reported in altered tuff layers from scattered localities around the world. Such tuff layers appear to be particularly associated with lacustrine deposits, where crandallite is formed by diagenetic processes at low temperatures, commonly involving percolating meteoric water (Flicoteau & Lucas 1984; Dill 2001). Phosphorus-enriched tuff layers have been described from Nova Scotia, Canada (Pe-Piper & Dolansky 2005), the Baltic countries (Kiipli *et al*. 2012), Poland (Kokowska-Pawlowska & Nowak 2013), Ellesmere Island, Canada (Reinhardt *et al*. 2013; von Gosen *et al*. 2019) and Czechia (Mach *et al*. 2021). Suggestions for the source of the phosphorus vary from dissolution of detrital apatite (Pe-Piper & Dolansky 2005) to eruption of a carbonatitic magma (Kiipli *et al*. 2012) and to deposition of organic matter during periodic climatic variations caused by cyclic orbital changes and accelerated by volcanic eruptions (Mach *et al*. 2021). Some papers do not offer an explanation at all.

Lacustrine mudstones and sandstones of Paleocene age occur in the Nuussuaq Basin on Qeqertarsuaq (Disko) and Nuussuaq, West Greenland (Fig. 1). They were deposited in successive lakes, which were partly dammed by

***Correspondence:** *lml@geus.dk*
Received: 27 Mar 2026
Revised: 22 Jun 2026
Accepted: 07 Aug 2026
Published: 25 Nov 2026

Keywords: bone, diagenesis, eruption, mass death, phosphorus-enrichment

Abbreviations
AQM: automated quantitative mineralogy
BSE: backscattered electron
EBF: Eastern Boundary Fault
EDX: energy dispersive x-ray spectroscopy
GEUS: Geological Survey of Denmark and Greenland
ICP-MS: inductively coupled plasma mass spectrometry
REE: rare-earth elements
TC: total carbon
TOC: total organic carbon
TS: total sulphur
XRD: x-ray diffraction
XRF: x-ray fluorescence spectrometry

GEUS Bulletin (eISSN: 2597-2154) is an open access, peer-reviewed journal published by the Geological Survey of Denmark and Greenland (GEUS). This article is distributed under a *CC-BY 4.0* licence, permitting free redistribution, and reproduction for any purpose, even commercial, provided proper citation of the original work. Author(s) retain copyright.

Edited by: Hyojin Kim (GEUS, Denmark)

Reviewed by: Lutz Reinhardt (BGR, Germany), Vladislav Rapprich (Czech Geological Survey, Czech Republic)

Funding: See page 21

Competing interests: See page 21

Additional files: See page 21

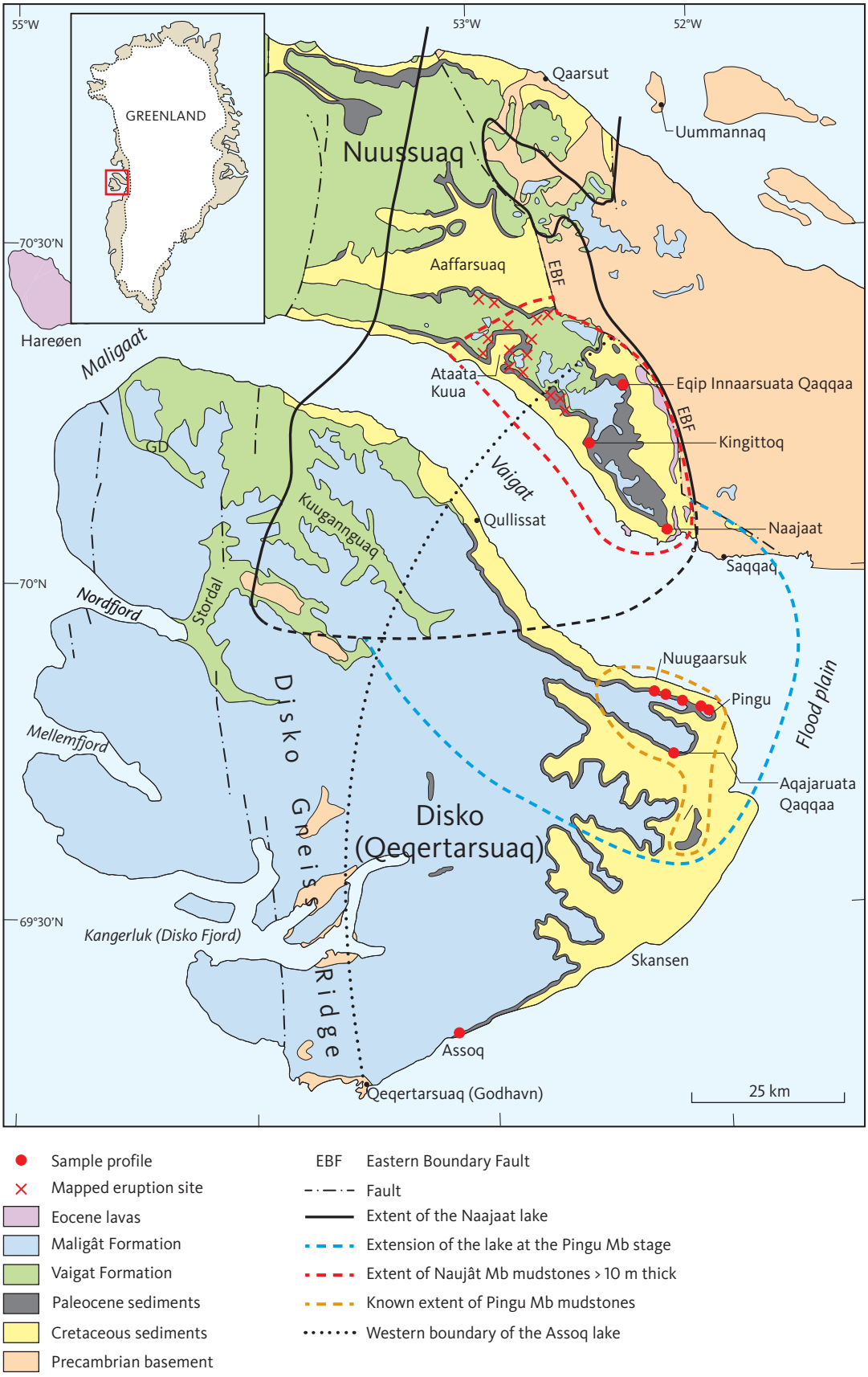

Fig. 1 Simplified geological map of Disko and Nuussuaq showing the extent of Naajaat Lake, which developed into the Pingu Lake, and the younger Assoq Lake. The mapped eruption sites of the Ordlingassoq Member are from Pedersen *et al*. (2007a).

advancing volcanic rocks (G.K. Pedersen *et al*. 1998). The mudstones contain a considerable number of tuff layers (up to 20 observed), which are pervasively diagenetically altered to crandallite-dominated mineral assemblages, though some layers can still be recognised as originally volcanic by the igneous textures of the clasts with pseudomorphs after olivine and plagioclase, and outlines of glass shards. In their present state, the layers contain up to 18 wt% P_2O_5 and down to 0.4 wt% SiO_2. In contrast, the surrounding sediments contain around 0.2 wt% P_2O_5 and 30–50 wt% SiO_2, and the contemporaneous volcanic rocks *c*. 0.1 wt% P_2O_5 and *c*. 49 wt% SiO_2 (Pedersen *et al*. 2017, 2018).

This study describes the phosphorus-rich tuff layers in the lake sediments of the Nuussuaq Basin and considers possible explanations for their formation.

2 Geological setting

The Nuussuaq Basin is a *c*. 120 km wide rift basin that extends for *c*. 400 km NNW–SSE along the coast of central West Greenland (e.g. Gregersen *et al*. 2019, 2022; Dam & Sønderholm 2021). Its eastern boundary towards the Precambrian basement is a large fault (the Eastern Boundary Fault, EBF) which runs NW–SE on central Nuussuaq and continues southwards east of Disko (Fig. 1). On Nuussuaq and Disko the basin fill consists of Cretaceous to Paleocene siliciclastic sedimentary deposits of the Nuussuaq Group (e.g. Dam *et al*. 2009) and Palaeogene volcanic rocks (e.g. Pedersen *et al*. 2017, 2018). A stratigraphic scheme for the part of the Paleocene relevant here is shown in Fig. 2. Eruption of the volcanic rocks of the Vaigat Formation started in western Nuussuaq at around 62 Ma (Storey *et al*. 1998) with deposition of submarine hyaloclastites and a subaerial lava plateau. A marine embayment was formed, bounded by the volcanic areas in the west and an irregular mountainous highland of Precambrian gneisses east of the boundary fault, and with a connection to the sea north of Nuussuaq (Pedersen *et al*. 1996). In this embayment, the synvolcanic marine mudstones of the Eqalulik Formation were deposited (Dam *et al*. 2009). Over time, the embayment became gradually more constricted as the volcanic areas expanded eastwards, and the advancing volcanic rocks of the Vaigat Formation (the Anaanaa and Naujánguit Members) were deposited in the embayment. At the end of deposition of the Naujánguit Member, the east-advancing volcanic rocks made contact with a large NW-extending gneiss promontory in northern Nuussuaq (notable in Fig. 1). Thereby the marine connection to the north became blocked, and the embayment was transformed into a freshwater lake (Pedersen *et al*. 1996). The non-marine sediments of the Atanikerluk Formation were deposited here in

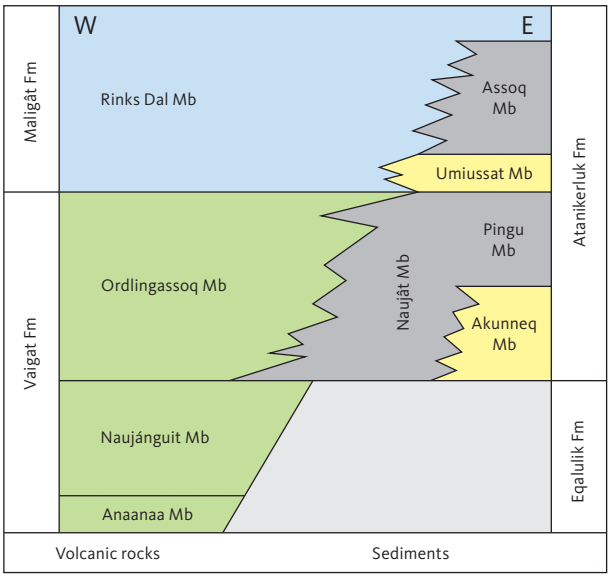

Fig. 2 Stratigraphy of the uppermost Danian to Selandian volcanic Vaigat and Maligât Formations and the contemporaneous sedimentary Eqalulik (marine) and Atanikerluk (non-marine) Formations and their members. The two upper members of the Maligât Formation (Nordfjord and Niaqussat Members) are not shown because at this stage the lakes were obliterated by the volcanic rocks. The figure illustrates schematically a NW–SE section approximately along the Vaigat Strait. Fm: Formation. Mb: Member.

three lacustrine stages with continuing infill of volcanic rocks of the Vaigat Formation (Ordlingassoq Member) and the overlying Maligât Formation (Rinks Dal Member) from the west and fluvial sand and mud from the east and south-east (Fig. 2; Pedersen *et al*. 1998; Dam *et al*. 2020).

3 Lakes of the Atanikerluk Formation

The blockage of the connection to the sea in the north caused the water level in the newly formed lake to rise above sea level. This resulted in the creation of a considerable accommodation space in the lake, as shown by the foreset-bedded hyaloclastite deposits which attained heights of up to 400 m in the central parts of the lake in southern and central Nuussuaq (Pedersen *et al*. 1993, 2002) and up to 500 m in northern Nuussuaq (Pedersen *et al*. 2006). The river draining the lake is considered to have been to the north of Nuussuaq, and the inlet was via one or two large rivers to the south-east, which presumably drained large parts of the interior of Greenland (Dam *et al*. 2020; Dam & Sønderholm 2021). The climate during the Paleocene was warm-temperate, based on fossils such as dinoflagellates (e.g. Nøhr-Hansen 2025).

3.1 Naajaat Lake and Naujât Member

The oldest lake was the Naajaat Lake in which the Naujât Member (old spelling retained) was deposited (Figs 1, 2).

To the north, the lake was constricted between the lava plateau in the west and the gneiss highland in the east. The position of its eastern boundary was probably relatively constant towards the steep Precambrian highland. The position of its western boundary fluctuated with the progradation of the volcanic rocks of the Ordlingassoq Member into the lake and variable water levels in the lake. This is illustrated by two 6–10 km long (in the E–W direction) wedges of hyaloclastite with east-dipping foresets interdigitating with subaerial lava flows (Pedersen *et al*. 1993, 2002, 2006). The western foresets are up to 100 m high, and the wedges thicken towards the east where they merge into 200–500 m thick deposits in the central part of the lake. To the south-west, similar hyaloclastite deposits are banked up against Precambrian gneiss in an emergent part of the Disko Gneiss Ridge (Fig. 1). To the south-east, the feeding river deposited the coarse, sandy fractions of its load onto a flood plain (the Akunneq Member, Figs 2, 3), which is exposed in easternmost Disko (Dam *et al*. 2009). Because of an almost complete lack of exposures along most of the north-eastern coast of Disko, the southern and south-eastern lake shoreline shown in Fig. 1 is inferred.

The Naujât Member comprises mainly dark grey, silty mudstones as described by Koch (1959) and G.K. Pedersen *et al*. (1998). The member is only a few metres thick in the western part of the lake, where the lake water was displaced at an early stage by hyaloclastites of the Ordlingassoq Member. In the central part of the lake where the water was 200–400 m deep, the Naujât Member is up to 230 m thick. In northern Nuussuaq, the member is not visible on aerial photographs, and relevant fieldwork has not been carried out.

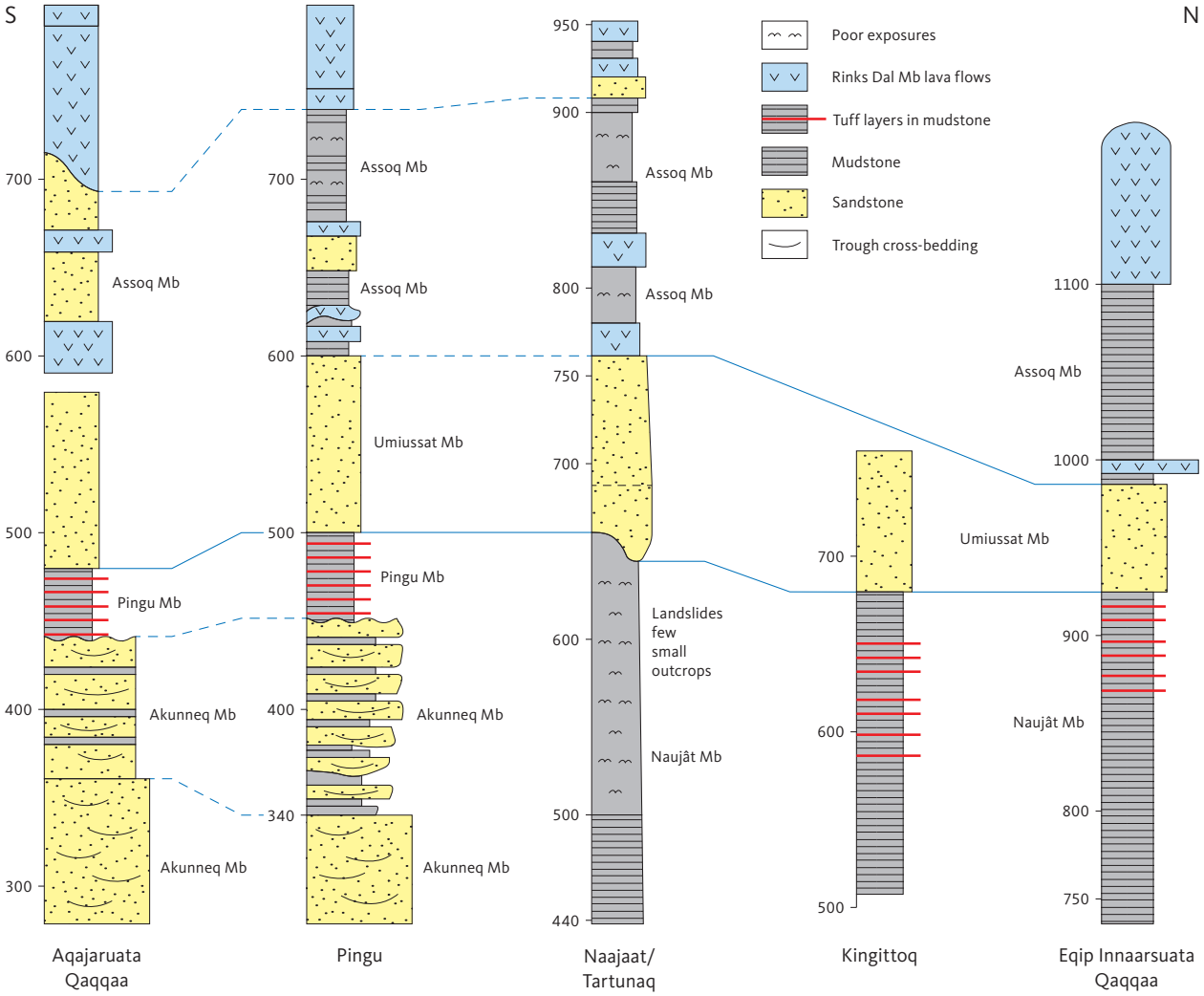

Fig. 3 Overview logs through the members of the Atanikerluk Formation in eastern Disko and Nuussuaq, showing how the Pingu Member correlates to the upper part of the Naujât Member, whereas the Akunneq Member correlates to the lower part of the Naujât Member. The logs are arranged in an S–N 'panel' from Disko to Nuussuaq. Log locations are shown in Fig. 1. The stratigraphy is aligned on the level of the Cretaceous–Palaeogene boundary, which represents a hiatus of around 33 million years (94–61 Ma; Dam & Sønderholm 2021). The lower lava flows of the Rinks Dal Member are invasive into the contemporaneous sediments (Pedersen *et al*. 2018). Numbers on the left side of the logs are metres above sea level. The increase in altitude from S to N is caused by post-volcanic tilting of the whole area towards SSE (Larsen & Pedersen 1992). Mb: Member.

A few layers of tuff occur in the basal part of the Naujât Member, but tuffs are otherwise absent in the lower part of the member. Tuff layers are frequent in the upper part of the member (the 'middle unit' of G.K. Pedersen *et al*. 1998), where several logged sections contain up to 20 tuff layers in over 30–50 m of stratigraphy (G.K. Pedersen *et al*. 1998). No tuff layers have been observed in the western, thinner part of the member, but as exposures of the mudstones here are commonly poor or non-existent, the presence of tuff layers cannot be excluded.

3.2 Pingu Lake and Pingu Member

The Naajaat Lake developed into the Pingu Lake by a rise in the lake level, possibly caused by further blocking of the outlet at higher altitudes by the east-advancing lava flows. As a result, the lake area expanded significantly to the south-east (Fig. 1). The Pingu Member comprises a succession of mainly dark grey, silty mudstones in eastern Disko, most commonly 40–60 m thick but reaching up to 85 m. It is well exposed over 14 km in the coastal section from Pingu in the east to Nuugaarsuk in the west (Fig. 1; Pedersen *et al*. 2005). The Pingu Member overlies fluvial plain deposits of the Akunneq Member and is correlated to the upper part of the Naujât Member (Figs 2, 3; Dam *et al*. 2009, figs 128, 131, 132). Like the upper part of the Naujât Member, the Pingu Member contains several tuff layers, and both are overlain by the sandy Umiussat Member succeeded by mudstones of the Assoq Member. The fluvial, sand-dominated Akunneq Member underlying the Pingu Member is thus time-equivalent to the lower part of the Naujât Member (Fig. 3).

Both the Naujât and Pingu Members become sandier in their upper parts, indicating fluvial progradation and shallowing of the lake. Around the same time, the volcanism of the Vaigat Formation came to an end.

3.3 Assoq Lake and Assoq Member

The time lapse between the end of the volcanism of the Vaigat Formation and the start of the volcanism of the Maligât Formation at around 60 Ma is unknown but thought to be probably less than a million years (Storey *et al*. 1998). Extrusion of the basalts of the Maligât Formation started in western Disko, and at that time a lake existed east of the Disko Gneiss Ridge and in southern Nuussuaq, where mudstones and sands of the Assoq Member were deposited. The Assoq Lake was confined to the north and west by volcanic deposits and the Disko Gneiss Ridge, and to the north-east by the gneiss highland on Nuussuaq (Fig. 1). The water was partially brackish, probably because of periodic ingress of the sea from the south. The Assoq Lake was gradually filled in from the west with hyaloclastites and subaqueous and invasive lava flows of the Rinks Dal Member of the Maligât Formation and was eventually obliterated (Fig. 3; Pedersen *et al*. 2018, fig. 16).

Tuff layers in the Assoq Member are rare. Despite reasonable exposures in eastern Disko, tuff layers have only been observed at Assoq in the southern part of the island.

3.4 Source of the tuff layers

The picritic to basaltic magmas of the Ordlingassoq Member of the Vaigat Formation were erupted from several sites exposed in southern Nuussuaq (Fig. 1). Many eruptions took place within the Naajaat Lake, building thick mounds of hyaloclastite deposits (see photogrammetric sections of Pedersen *et al*. 1993, 2007b). Such hydromagmatic eruptions invariably created ash clouds and tuff deposits in the surrounding areas, even though the magmas were not volatile-rich. The tuff-bearing localities on Nuussuaq are situated 5–30 km from the known eruption sites (Fig. 1), whereas tuff localities on Disko are situated 50–60 km from these eruption sites.

The easternmost exposure of the Ordlingassoq Member is a large picrite sill within Cretaceous sediments exposed over *c*. 7 km to the north, east and south of Eqip Innaarsuata Qaqqaa. The sill is shown on the geological map of Pedersen *et al*. (2007a). It is more than 15 m thick (AKP, unpublished field notes 2004) and considered to be an invasive lava flow underlying the entire Eqip Innaarsuata Qaqqaa massif. The sill is important for the interpretation of the mineralogy of the tuffs in the nearby sample profile, as discussed later.

The basaltic magmas of the Rinks Dal Member of the Maligât Formation erupted mostly subaerially, and such eruptions would not have created notable tuff deposits, explaining the rarity of tuff layers in the Assoq Member. However, the Assoq Lake was filled from west to east by successive hyaloclastites which mostly originated from subaerial flows that erupted in western Disko, and, flowing eastward, entered the Assoq Lake east of the Disko Gneiss Ridge (Larsen *et al*. 2006; Pedersen *et al*. 2018, their fig. 16). Some eruptions also appear to have taken place within the lake itself. The associated hydromagmatic explosions likely resulted in the formation of tuff layers such as those found at Assoq in southern Disko (Dam *et al*. 2009, their fig. 139).

There is thus no doubt that the tuffs originated from the voluminous magmas, which were in part erupted directly into the lakes. The compositions of these magmas, and thereby the original compositions of the tuffs, are well known (Pedersen *et al*. 2017, 2018).

4 Materials and methods

Samples of mudstones and tuff layers were collected during fieldwork in 1986–1988. Logging and sampling

were done mainly in profiles, with spacing between samples dependent on lithological variations and frequency of tuff layers (Fig. 4). Most observed tuff layers were sampled. These layers have sharp lower boundaries and more diffuse upper boundaries and are normally graded; these characters are specific to airfall tuffs, including tuffs that have settled through a water column (Fisher & Schmincke 1984). The layers are located up to 60 km from the eruption sites and cannot be toesets of the crater-near hyaloclastite deposits centred around Ataata Kuua (Fig. 1).

The tuff samples are friable, and the thin sections made in 1986–1988 could not be polished. Five new thin sections were made in 2024 by Pelcon Materials and Testing ApS, Copenhagen, Denmark. The samples were repeatedly embedded in yellow epoxy and precision-ground and -polished to a thickness of 20 µm.

Most samples were analysed by x-ray diffraction (XRD) by E. Leonardsen (1987–1993; spectra recorded on paper) at the Geological Institute, University of Copenhagen, Denmark. Some repeat analyses were made in 2024 and 2026 at the Department of Geosciences and Natural Resource Management, University of Copenhagen, using a monochromatic Bruker AXS D8 advance powder diffraction instrument with a copper source (Cu 1.5406Å) and a LynxEYE detector, a stepsize of 0.02°, a divergence slit of 0.443, and a measurement time on a rotating stage of 4 sec/step (8 sec/step for sample 323281 to obtain a better signal-to-noise ratio).

Backscattered Electron (BSE) imaging and Energy Dispersive X-ray Spectroscopy (EDX) analyses were conducted using a Zeiss Sigma 300VP SEM Scanning Electron Microscope at GEUS, equipped with two Bruker XFlash 6|30 EDX detectors, with 129 eV energy resolution. The same instrument was used to perform Automated Quantitative Mineralogy (AQM) analyses with the Zeiss Mineralogic™ software platform, which integrates BSE images with EDX analyses. It enables semi-quantitative analysis of chemical compositions, mineral phases and phase associations. For the AQM analysis, a mosaic of overlapping BSE images was defined. BSE images were acquired under high vacuum conditions with an aperture size of 120 µm and an acceleration voltage of 15 kV. Within the BSE images, a grid of EDX analytical points with a user-defined step size of 5–20 µm, was created. The EDX spectra are fully deconvoluted for each analysis, including matrix corrections, and therefore return the chemistry in wt% for each analytical point. Mineral identification was based on user-defined phase lists, where each phase was characterised by elemental boundaries and assigned a unique colour. These lists were applied to all EDX data to generate mineral and element maps

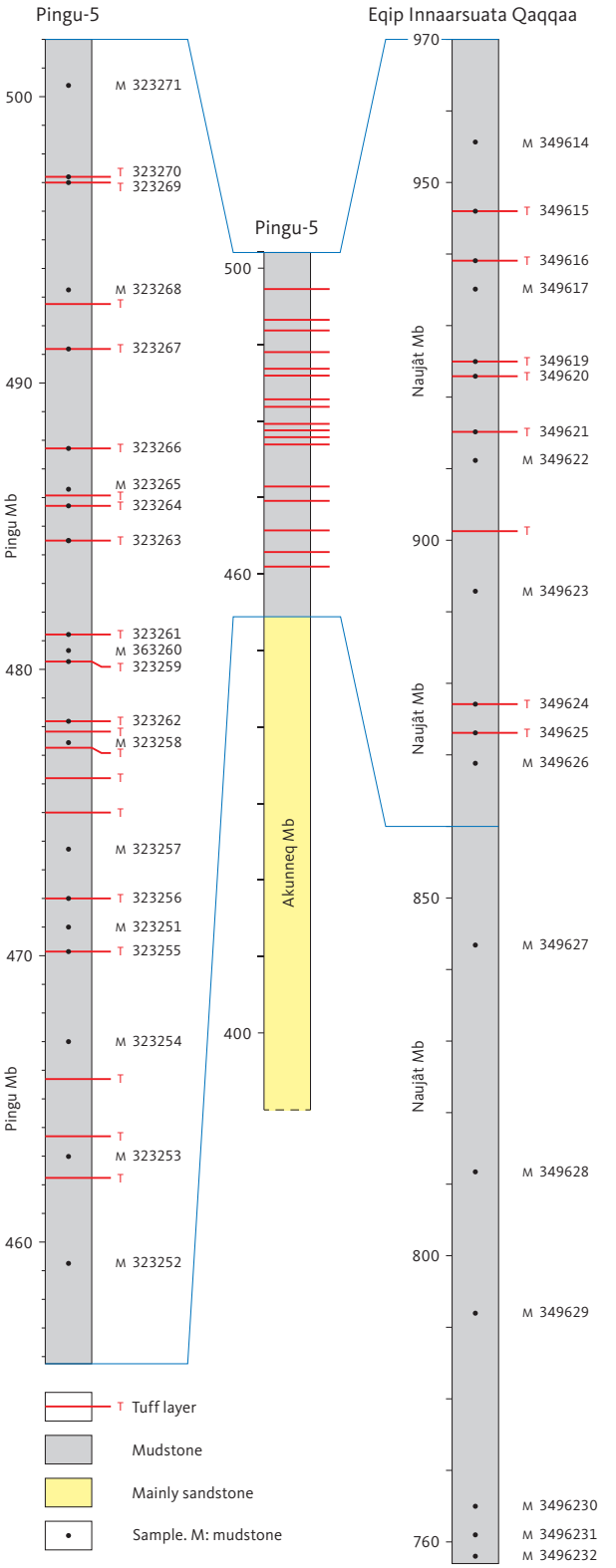

Fig. 4 Detailed logs of the two profiles with the most investigated samples. The Eqip Innaarsuata Qaqqaa profile is located on Nuussuaq at 70°15.83'N, 52°19.6'W, and the Pingu-5 profile is located on Disko at 69°47.21'N, 52°03.0'W (locations in Fig. 1). The Pingu-5 profile in the middle is drawn at the same scale as the Eqip Innaarsuata Qaqqaa profile, whereas the detailed Pingu-5 profile to the left is four times enlarged relative to the two others. Mb: Member.

in the AQM software (see Keulen *et al*. 2020 for more details). The Zeiss Mineralogic software was also used to make element maps for some of the major elements in the sample. All EDX analyses are semi-quantitative. Due to the very small grain sizes (clay fraction), the intimate mineral intergrowths and the OH-rich character of most minerals, many mineral analyses represent mixtures and are only partial; nonetheless, the measurements are sufficient to identify the phases present but are not published here.

Petrographic examination of sample 323281 was carried out in white reflected light and blue light illumination using oil immersion and a Zeiss incident light microscope, to document the presence of organic matter. Random reflectance (R_o) measurements were made on huminitic particles using a Leitz incident-light microscope fitted with the Discus-Fossil system (Hilgers Technisches Büro, Germany) and a 50× oil immersion objective lens. Calibration of the microscope system was assessed using a YAG 0.903% R_o calibration standard with integrated optical zero standard. The mean R_o was calculated from the measured reflectance values.

Selected samples were analysed for major elements by x-ray fluorescence (XRF) spectrometry by I. Sørensen and J. Kystol at the Geological Survey of Greenland (GGU) and its successor, GEUS (since 1995), following the methods described by Kystol & Larsen (1999). Trace elements were analysed by XRF by J. Bailey at the Geological Institute, University of Copenhagen, and later by inductively coupled plasma mass spectrometry (ICP-MS) by J. Kystol at GEUS, following methods described by Ottley *et al*. (2003). Total carbon (TC) and total sulphur (TS) analyses were made by D. Kiel-Dühring at GEUS using a LECO-200 instrument. Total organic carbon (TOC) analyses showed anomalously low values, probably because humic substances were dissolved during the analytical acid treatment, and these results are not reported. Many samples do not contain any carbonate, and in these, all the carbon is organic.

5 Results

5.1 Field work

Overview logs through the members of the Atanikerluk Formation are shown in Fig. 3, and the two profiles with the most investigated samples are shown schematically in Fig. 4. At the start of the field work, it was expected that a tuff stratigraphy with numbered layers could be established and used for lateral correlation, as done for the Eocene tuff layers in Denmark (Bøggild 1918). However, the absence of recognisable marker layers prevented this.

The tuff layers are 0.5–3 cm thick, commonly around 1 cm. On exposed surfaces in the field, the tuff layers weather white, which makes them easily visible against the dark grey mudstones. Fresh tuff fragments have a light brownish-orange colour (Fig. 5). Most tuff layers have a uniform appearance in the field, but grain-size variations and double layers have been observed. The tuff layers are slightly harder than the surrounding mudstones but are fragile and break easily. Most collected tuff samples consist of a collection of fragments of the tuff layer with attached, somewhat hardened, adjacent mudstone a few millimetres thick (Fig. 5). The analysed mudstone samples were taken well away from the tuff layers (Fig. 4).

5.2 Petrography of the phosphorus-rich tuff layers

5.2.1 Structures

Under the microscope, the dominant colour of the tuff is brownish orange, whereas the hardened adjacent mudstone is brownish black (Fig. 6). Lower boundaries are relatively sharp, whereas upper boundaries are more diffuse. Close to the boundaries, 'wispy' streaks of mudstone material may extend into the tuff layer (Fig. 6, 349620). Layers in which large volcanic clasts are distinguishable have wavy lower boundaries deformed by clasts (Fig. 6, 323281). Structures resembling burrows are seen in the lower part of one tuff layer (Fig. 6, 349621) and below one tuff layer (see SEM-AQM analysis traverses for sample 349620 in Section 5.2.2 Mineralogy).

Almost all tuff layers are normally graded. Most of the thinner layers consist of a single fining-upwards layer (Fig. 6, 323267, 349620), whereas some of the thicker layers comprise two (Fig. 6, 323256, 323281), rarely three (Fig. 6, 349621) fining-upwards layers with internal boundaries interpreted to reflect deposition



Fig. 5 Fragment of tuff layer, sample GGU 323275, Nuugaarsuk, Disko. The pale orange-brown tuff layer is 12 mm thick to the right; to the left, the upper part is missing. Note the sharp boundaries to the adjacent black mudstone.

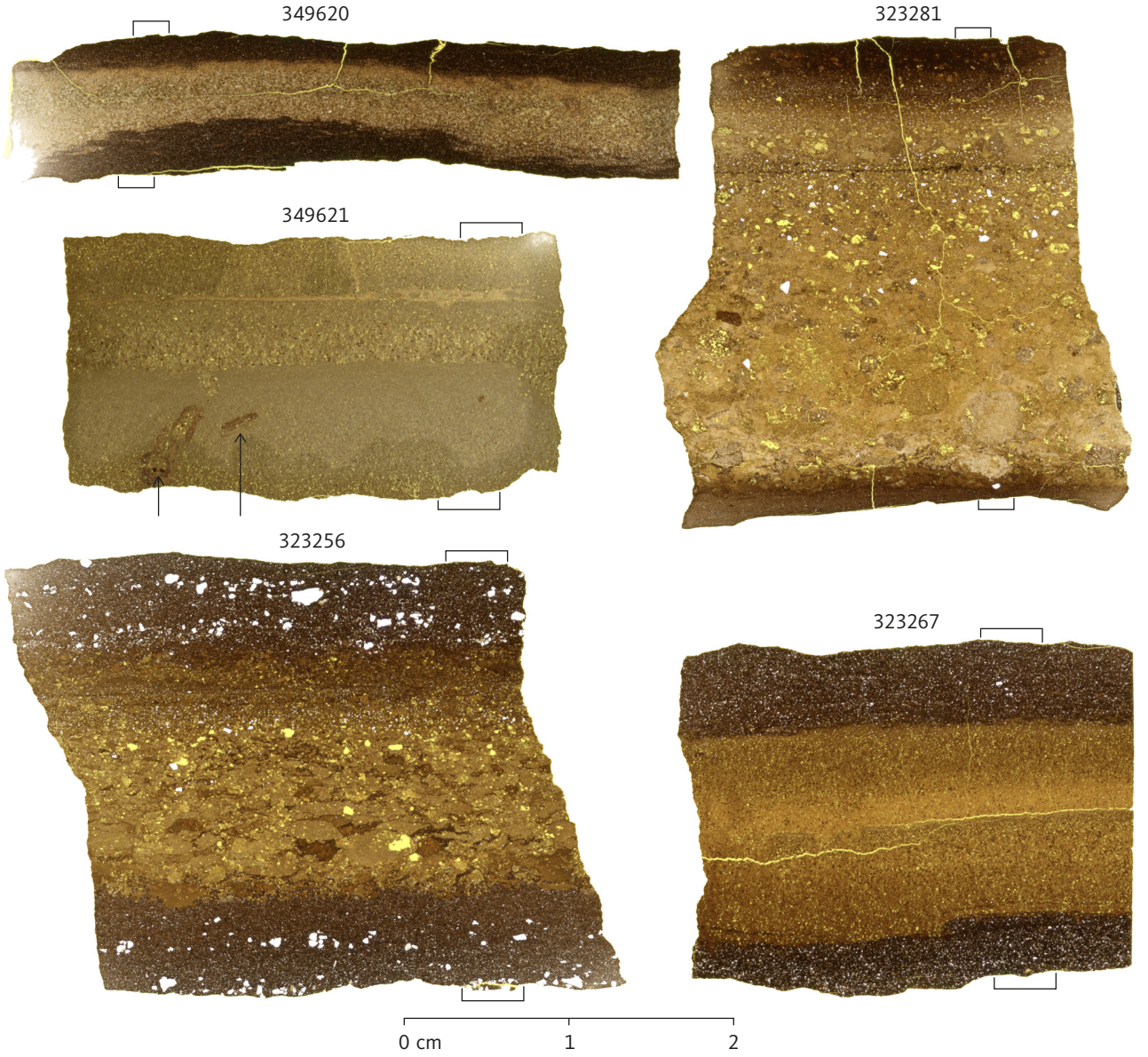

Fig. 6 Thin sections (20 µm thick) of tuff layers, all arranged with the stratigraphic base down and the top up (locations in Fig. 4). The crandallite-rich tuff layers are distinctly brown despite the thinness of the sections. The black adjacent mudstones are present both above and below the tuff in all but sample 349621, which has no mudstone preserved. **Pale yellow** areas represent pore spaces and cracks. Quartz grains are **white**; note the presence of quartz grains, fining upwards, in the upper half of the tuff in sample 323281. Several recognisable volcanic clasts are seen in sample 323281, where they are rounded, and in sample 323256, where they are flattened. Two arrows point to two tube-like features near the base of sample 349621, which may represent burrows. Square brackets at section margins indicate the positions of the SEM traverses shown in Figs 12, 14 and Supplementary Files S2–S4.

in successive pulses. Angular to subrounded quartz grains of clastic origin are present in the upper parts of the tuff layers from the Pingu Member; they increase in frequency and decrease in grain size towards the top of a layer (Fig. 6, sample 323281). Such quartz grains are not present in the tuff layers from the Naujât Member.

Remnants of volcanic clasts are found in the thicker tuff layers from the Pingu Member but only in two layers from the Naujât Member. Sample 323281 contains the best-preserved clasts (Figs 6–8). They are mostly rounded to lobate, and the largest, up to 4 mm in diameter, are situated near the layer base. Igneous textures showing outlines of olivine, plagioclase and pyroxene are preserved (Fig. 7), testifying to the volcanic origin of the tuff layers. Cruciform quench-crystal forms of original titanomagnetite are preserved but now consist of a secondary TiO_2-phase (Fig. 8A). Another sample, 323256, contains lobate to angular, somewhat flattened brown clasts, consistent with altered volcanic glass, up to 5 mm in length at the base of the layer (Fig. 6) and with clasts distinctly fining upwards. Most brown clasts appear homogeneous, while a few display possible remnant igneous textures

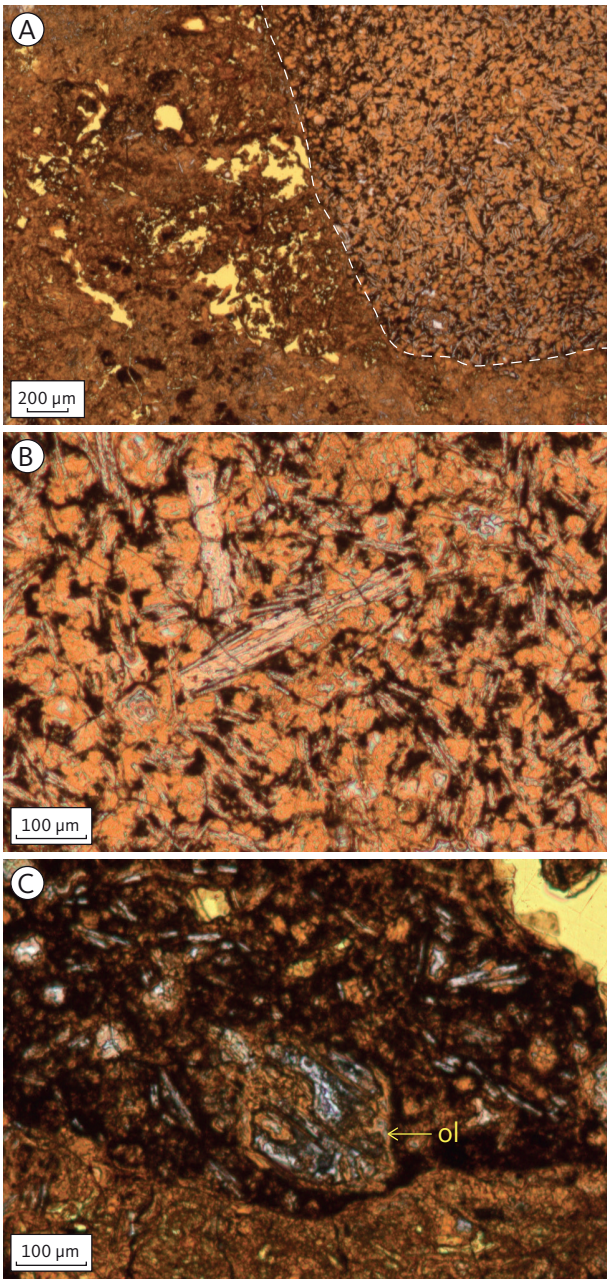

Fig. 7 Microphotographs (transmitted light) of volcanic clasts with preserved igneous textures, all from sample 323281. **A**: The right part of the photo shows part of a 4 mm diameter rounded clast (bounded by a **white dashed line**) situated near the base of the layer in the middle right-hand part of the thin section in Fig. 6. The clast presents the texture of a basalt with plagioclase laths, isometric grains of pyroxene and olivine, and interstitial oxides. The left part of the photo shows the tuff matrix with pore spaces (**yellow**) and faint traces of small black, vesicular grains (100–200 µm across) in a brown matrix. All silicates are altered to crandallite, and primary Fe-Ti oxides are altered to oxidised and hydrated Fe phases and oxidised Ti phases. **B**: Close-up of the igneous texture in the 4 mm clast in A: Light 'plagioclase' laths (two microphenocrysts and several groundmass laths), **darker orange** 'pyroxene' and 'olivine' grains and **brownish-black** interstitial 'Fe-Ti oxides' and residuum. All silicates are replaced by crandallite, and the oxides are oxidised and hydrated. **C**: An igneous clast *c*. 1 mm across with a pseudomorph of a lozenge-shaped microphenocryst of olivine (**ol**) and microlites of **light** 'plagioclase', **orange** 'olivine' and 'pyroxene' in a **black** groundmass of altered glass. The **whitish** patches inside the pseudomorphosed olivine are secondary apatite, and the rest is Fe-Ti-stained crandallite.

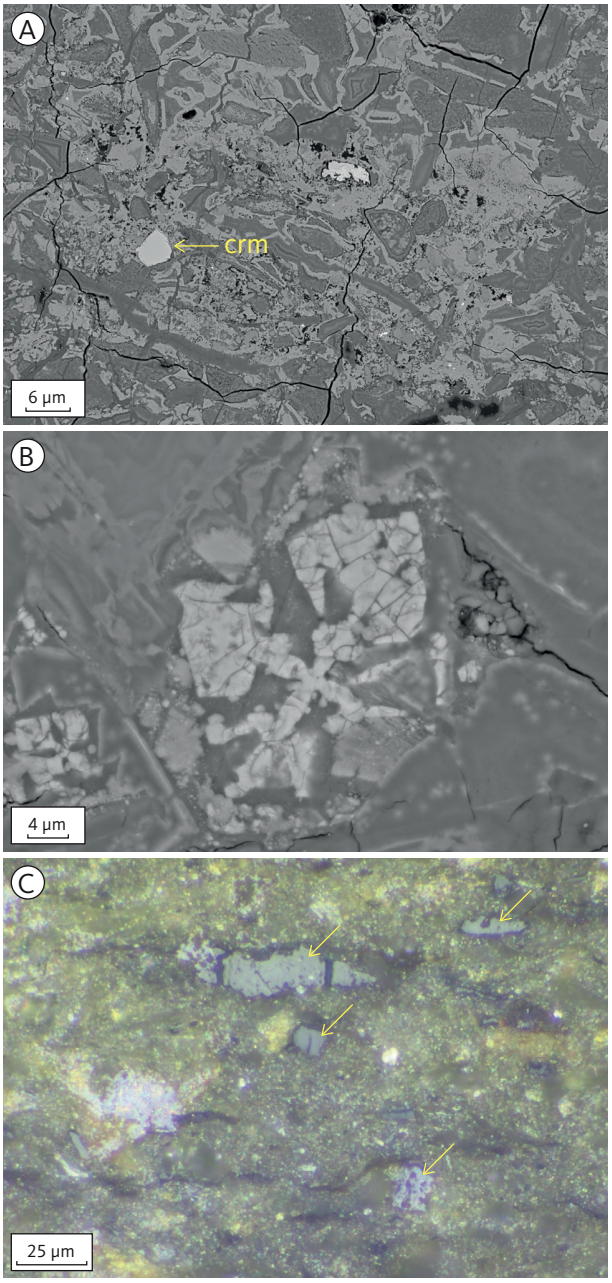

Fig. 8 Imaging of sample 323281. **A**: Backscattered electron image of an igneous clast containing a near-euhedral chromite crystal with unaltered high-temperature composition (**crm**). The white grain in the upper middle portion is pure Fe-oxide or hydroxide. No igneous textures are discernible, and the clast consists mainly of intergrown crandallite (**dark grey**) and apatite (**medium grey**). **B**: Backscattered electron image of the interstitial part of the large clast shown in Fig. 7A. The original titanomagnetite was quenched at high temperature, resulting in a characteristic cruciform skeletal growth (Haggerty 1976, p. Hg-106–Hg-108). The mineral now consists of a poorly defined Ti-oxide phase (**light grey**). The surrounding original glass is replaced by crandallite (**dark grey**). **C**: Reflected-light image (white light, oil immersion), showing organic carbon (**grey**, **yellow arrows**) filling interstices. Several carbon particles in this sample show evident plant cellular structure; in this image, the carbon particle in the lower right part.

with traces of tiny, < 0.07 mm, colourless laths. The larger clasts are embedded in a matrix of finer-grained glass shards, which dominate in the upper part of the layer. No glass is preserved.

Samples without larger clasts consist of close-lying small grains < 0.2 mm across, fining upwards to < 0.1 mm, and commonly with sharp-edged outlines consistent with an origin as glass shards (Fig. 9A).

Some samples contain scattered 'ovoids' filled with late-grown minerals in a concentric pattern (Fig. 9D); it is not possible to tell whether these were originally vesicles. All samples have many pore spaces of which some are open (Fig. 7A), others are filled with carbon (Fig. 8C). However, the BSE images cannot distinguish between open and carbon-filled pores. One organic-looking feature in sample 323267 is identified as a funginite (Fig. 10D).

All tuff layers display evidence of having, to a large extent, originally consisted of volcanic glass fragments, but with one exception (chromite), all glass and igneous minerals have been replaced.

5.2.2 Mineralogy

Nearly all samples of mudstone and tuff layers have been analysed by XRD. These analyses show that crandallite is a major constituent of all the tuff layers from the Naujât and Pingu Members. A diffractogram of a crandallite-rich tuff layer is shown in Fig. 11. Moreover, crandallite does not occur in the mudstones except for the few millimetres of diagenetically hardened mudstone in direct contact with the tuff layers. The crandallite is thus uniquely associated with the tuffs.

Thin sections of the tuff layers are difficult to study in transmitted light because of the extremely small grain size and heavy iron staining. Consequently, element maps and AQM mineral maps were made by SEM in traverses across the five thin sections shown in Fig. 6. Results for two samples are shown in Figs 12–14 (legend in Fig. 13), and results for the other three samples are shown in Supplementary Files S2–S4. The mineralogy of tuffs and adjacent mudstones calculated separately is shown in Table 1. In the AQM maps, carbon appears together with the pore spaces as 'holes'. Examination under a reflected-light microscope revealed the frequent presence of irregular masses of

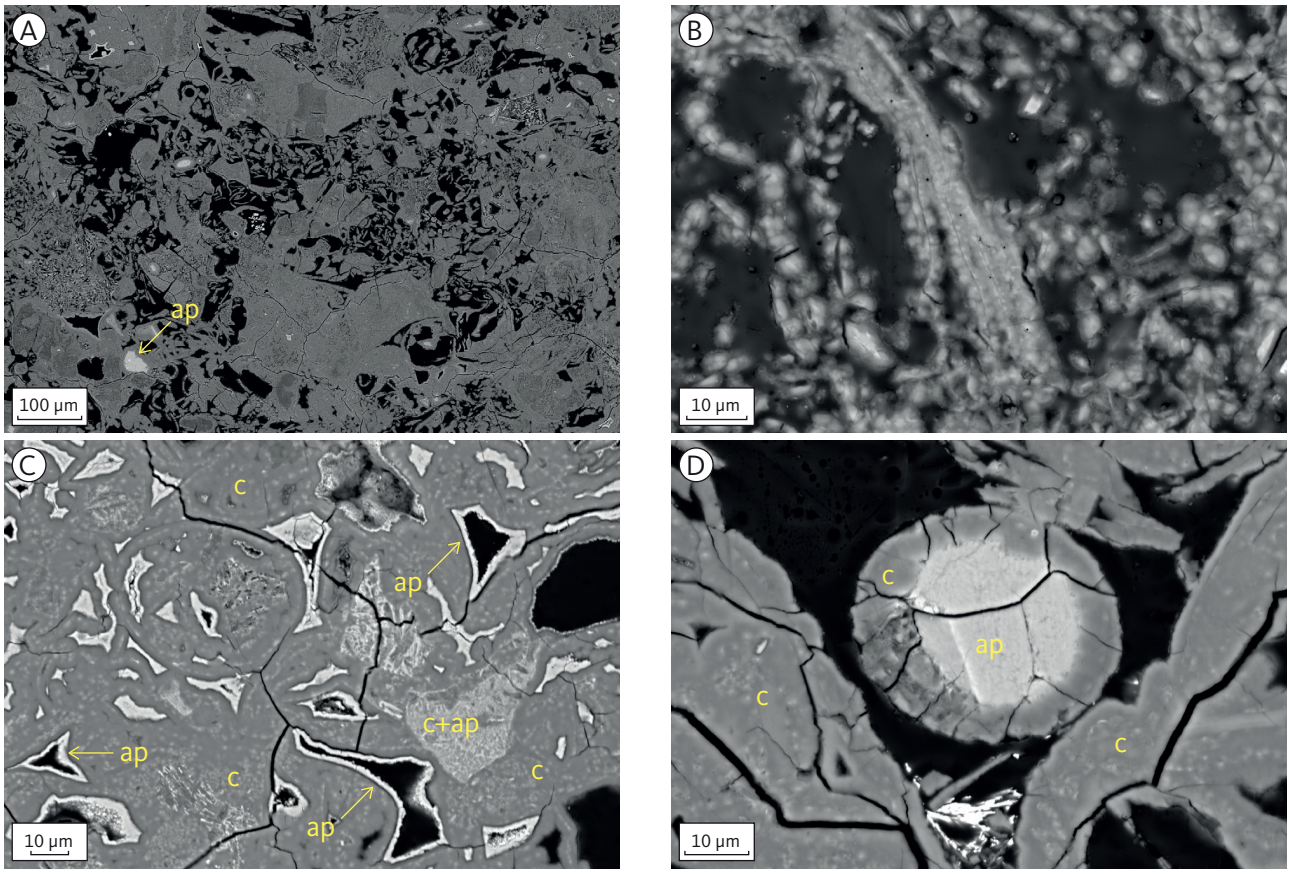

Fig. 9 Backscattered electron images. **A**: Overview of the tuff structure with sharp-edged glass shards and splinters, now all replaced by crandallite. The white grains are late apatite (**ap**). Note the frequent black pore spaces, which seem to be open although many are filled with carbon, which is 'invisible' to the SEM. Sample 323267. **B**: Crandallite crystallised in characteristic spherules and strings of spherules forming fibres, surrounded by pore spaces. Sample 323256. **C**: Crandallite matrix (grey, **c**) with interstitial pore spaces lined or filled with apatite (white, **ap**) – but note nearly unlined pores to the right. Two light grey grains in the right half of the image are intergrown crandallite, apatite and Fe-Ti oxides or hydroxides (**c+ap**). Sample 323267. **D**: Crandallite matrix (grey, **c**, with traces of spherules) and angular pore space (black) with an ovoid lined with crandallite (**c**) and filled with apatite (light grey, **ap**). The small white needles near the base of the image are an iron oxide. Sample 323267. Irregular cracks in (**C**) and (**D**) are desiccation cracks induced in the SEM instrument.

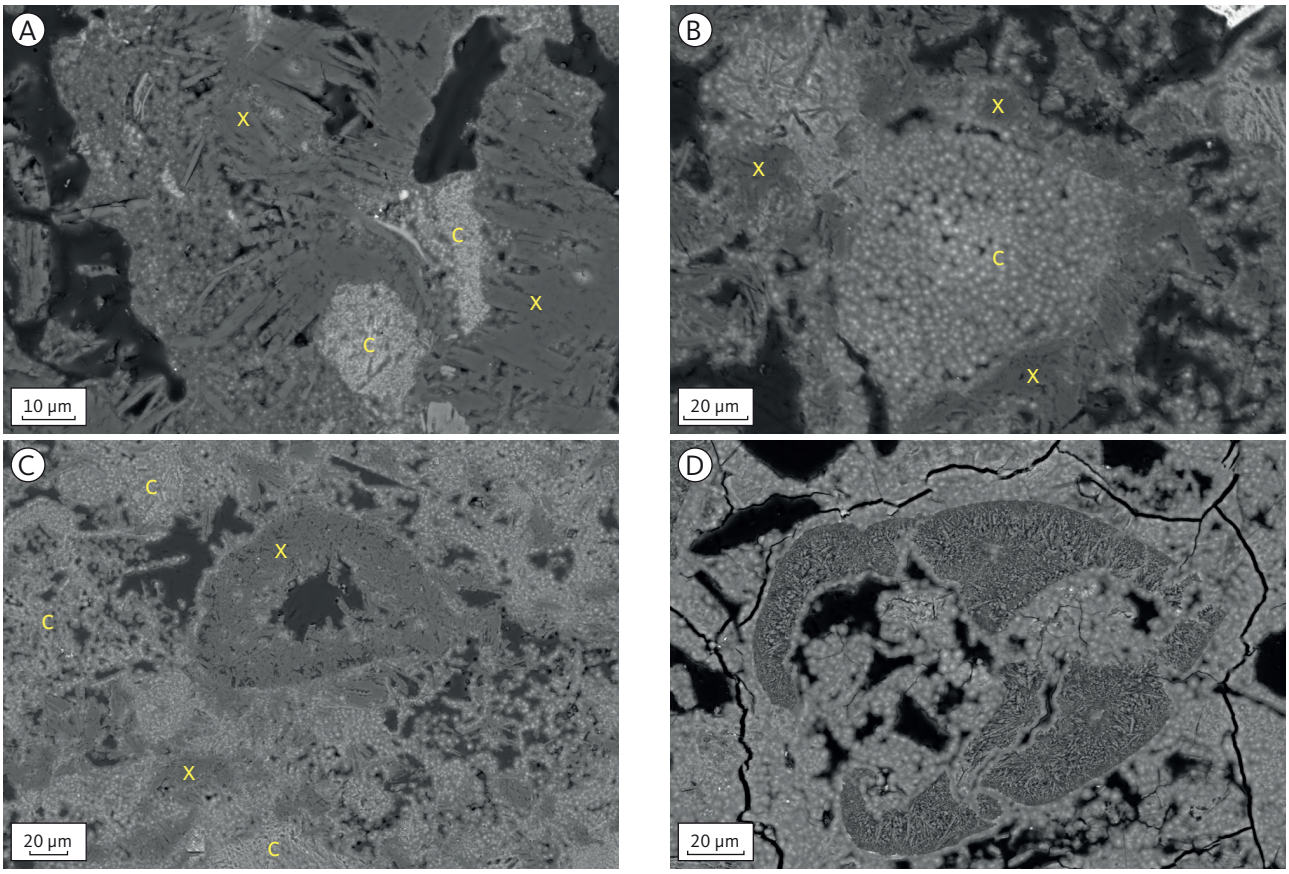

Fig. 10 Backscattered electron images. **A**: Intergrown mineral X (**x**) and crandallite (**c**). Two large, light grey, inhomogeneous areas are mainly crandallite. Mineral X forms the dark grey material with a fibrous structure; the small light patches within the fibres are crandallite. The black areas are pore spaces. Sample 349620. **B**: White-speckled spherulitic crandallite 'grain' (**c**) with rim of dark grey mineral X (**x**) growing into pore spaces. Sample 349621. **C**: The matrix consists of intimately intergrown white-speckled crandallite (**c**) and dark grey mineral X (**x**). An ovoid cavity is partly filled with mineral X and only a little crandallite. The black areas are pore spaces. Sample 349621. **D**: Organic-looking feature with bilateral symmetry interpreted to be a funginite, the reproductive organ of a fungus (ICCP 2001). Its original form was an ovoid with two round chambers; it is now slightly squashed and broken. Both matrix and funginite now consist entirely of crandallite. The crandallite matrix has the characteristic spherulitic texture, whereas the crandallite replacing the funginite is more fine-grained and fibrous. Sample 323267.

organic carbon, some of which have preserved plant cellular structures (Fig. 8C).

The element maps for Si show how this element decreases from 15–20 wt% in the mudstones to close to 0% in the tuff layers. The mineral maps and Table 1 show that the tuff layer in sample 323267 consists predominantly of crandallite (86 area% in Table 1), and the tuff layer in sample 349620 consists of a mixture of around equal parts of crandallite and a mineral with very high Al content ('mineral X', see next paragraph). The adjacent mudstones are dominated by kaolinite, quartz and iron oxide or hydroxide. Notably, crandallite occurs dispersed in the immediately overlying mudstone but is rarely present in the underlying mudstone except in some sharply delimited areas, perhaps burrows, in sample 349620 (Fig. 14). The EDX analyses show that the crandallite grains contain considerable amounts of BaO (3–10 wt%) and SrO (2–5 wt%) in concentrations varying between individual grains in a sample. These elements represent the Ba- and Sr- analogues gorceixite and goyazite, which are in solid solution in the crandallite.

Combining all data, the present mineral assemblages in the tuff layers of the Naujât and Pingu Members comprise mainly crandallite (including mixtures up to nearly 90 area% in the SEM studies, Table 1) together with minor amounts of apatite and oxides or hydroxides of Fe and Ti and rare baryte. Scattered grains of quartz, kaolinite and K-feldspar are considered to represent mudstone minerals which ended up in the tuff layers during deposition. Kaolinite occurs more frequently in the upper layer of tuffs with two pulses (323256 and 323281, Fig. 6). In one profile on Nuussuaq (Eqip Innaarsuata Qaqqaa) the tuff layers contain an unnamed nitrogen-bearing aluminium carbonate-hydroxide mineral, which we here denote 'mineral X'. A full chemical and structural characterisation of mineral X is ongoing and beyond the scope of the present study.

Rare remains of the original igneous mineralogy comprise only a few grains of magnesian chromite (Fig. 8A) compositionally similar to the high-temperature quenched chromites in the picrites of the Vaigat Formation (Larsen & Pedersen 2000).

The mudstones consist of kaolinite, quartz, feldspars, illite and mixed-layer clays and, on Disko, commonly minor gibbsite and siderite (XRD data). G.K. Pedersen *et al*. (1998) describe the mudstones further.

5.2.3 Mineral textures

Because of the extremely fine-grained character of the tuffs, the very variable textures are best seen in BSE images taken in the SEM. At moderate magnifications, crandallite forms apparently compact masses with varying grey-scale colours, but at large magnification the mineral 'grains' are seen to consist of closely intergrown fibres and tiny (< 1 µm) spherules with light grey centres and darker rims. Many fibres also consist of strings of such spherules (Fig. 9B). Many strings and spherules appear to have grown freely into pore spaces (Fig. 9B). The varying grey tones of crandallite in the BSE images can in some cases be explained by varying contents of Ba, in other cases by intergrowth with Fe-Ti hydroxides or oxides (Fig. 9C), and in some cases they are unexplained. Inside the volcanic clasts, crandallite appears to be more uniformly grey. In transmitted light, pseudomorphs of plagioclase laths are lighter than pseudomorphs of olivine and pyroxene (Fig. 7B), perhaps because the plagioclase had very small contents of iron available for incorporation into the crandallite.

Secondary apatite has replaced the centre of an olivine crystal (Fig. 7C) and occurs as late-formed linings of pore spaces (Fig. 9C) and as fill of a 40 µm round body (ovoid or fibre, Fig. 9D). Most apatite seems to have formed during a late-stage process.

In transmitted light, mineral X is colourless but very brown-stained and has high birefringence; it is uniformly dark grey in BSE images (Fig. 10). The mineral is as fine-grained as crandallite and exhibits fibrous growth forms like crandallite. Even massive-looking patches of mineral X consist of fibres when seen at larger magnification (Fig. 10A). Mineral X and crandallite may be intimately intergrown (Fig. 10A, C), crandallite may be rimmed by mineral X (Fig. 10B), and larger pore spaces may be partially filled with fibres of mineral X growing into the void (Fig. 10C). This indicates that mineral X crystallised together with and later than crandallite.

The AQM mineral maps of the tuffs measured 'holes' (pore spaces + carbon) to constitute 10–12 area% in four samples and 4 area% in one sample. The adjacent mudstones contain only 0.2–2.0 area% 'holes' (Table 1).

5.3 Tuff layers in the Assoq Member

Tuff layers from the Rinks Dal Member of the Maligât Formation deposited in the Assoq Lake at Assoq in southern Disko (Fig. 1) are 5–30 mm thick, greenish brown and consist of compressed glass shards, rounded ovoids and interstices with concave outlines. The glass is completely altered to greenish-brown clays, and the ovoids and interstices are lined with brown clay; some are filled with carbonate. These tuff layers contain no crandallite and are not enriched in phosphorus. Their composition corresponds to a strongly altered and hydrated basalt (chemical analyses in Supplementary File S1).

5.4 Chemical compositions

The XRF analyses of the tuff layers from the Naujât and Pingu Members show a range of SiO_2 contents (0.4–33.6 wt%). The high values are caused by the inclusion of mudstone in the analysed material, mainly from the adhering hardened adjacent mudstone. Comparison with the thin sections and the SEM analyses indicates that XRF analyses with more than around 10–15 wt% SiO_2 represent material which includes adjacent mudstone. Analyses with < 15 wt% SiO_2 represent tuff layers with gradational boundaries, wisps of adjacent mudstone (kaolinite) and detrital quartz grains within the tuff layer. The SEM compositional cross sections (Figs 12–14, Supplementary Files S2–S4) clearly show that the homogeneous tuff layers contain close to 0% SiO_2. Chemical analyses of tuff samples containing little to no adjacent mudstone are presented in Table 2. All tuff and mudstone analyses are in Supplementary File S1.

The tuff layers in the Naujât and Pingu Members contain up to 18 wt% P_2O_5 (Table 2), reflecting the high amounts of crandallite. The tuff layers are also strongly enriched in Ba (up to 19 800 ppm = 2.2 wt% BaO), Sr (up to 24 600 ppm = 2.9 wt% SrO) and rare-earth elements (REE; up to 550 ppm Ce). In contrast, the surrounding mudstones have around 40 wt% SiO_2, 0.2 wt% P_2O_5, 300–600 ppm Ba and 100 ppm Sr (Table 2 and Supplementary File S1). The Precambrian basement in the region contains around 0.1 wt% P_2O_5 and variable Ba and Sr, both around 100–1200 ppm (Pedersen *et al*. 2018, their table 13). Further, the tuff layers have total carbon contents of 4.5–10 wt%, average 8.3 wt%, slightly higher than in the surrounding mudstones with 2.8–10 wt% TC, average 6.6 wt% (Table 2; Supplementary File S1; G.K. Pedersen *et al*. 1998).

The original volcanic material of the tuff layers belongs to the Ordlingassoq Member and was basaltic to picritic in composition. It contained about 47–49 wt% SiO_2, 0.1–0.2 wt% P_2O_5, less than 100 ppm Ba and around 200 ppm Sr (Pedersen e*t al*. 2017, their table 6). The contents of carbon and water in the original glass would have been negligible due to degassing of the magma during eruption.

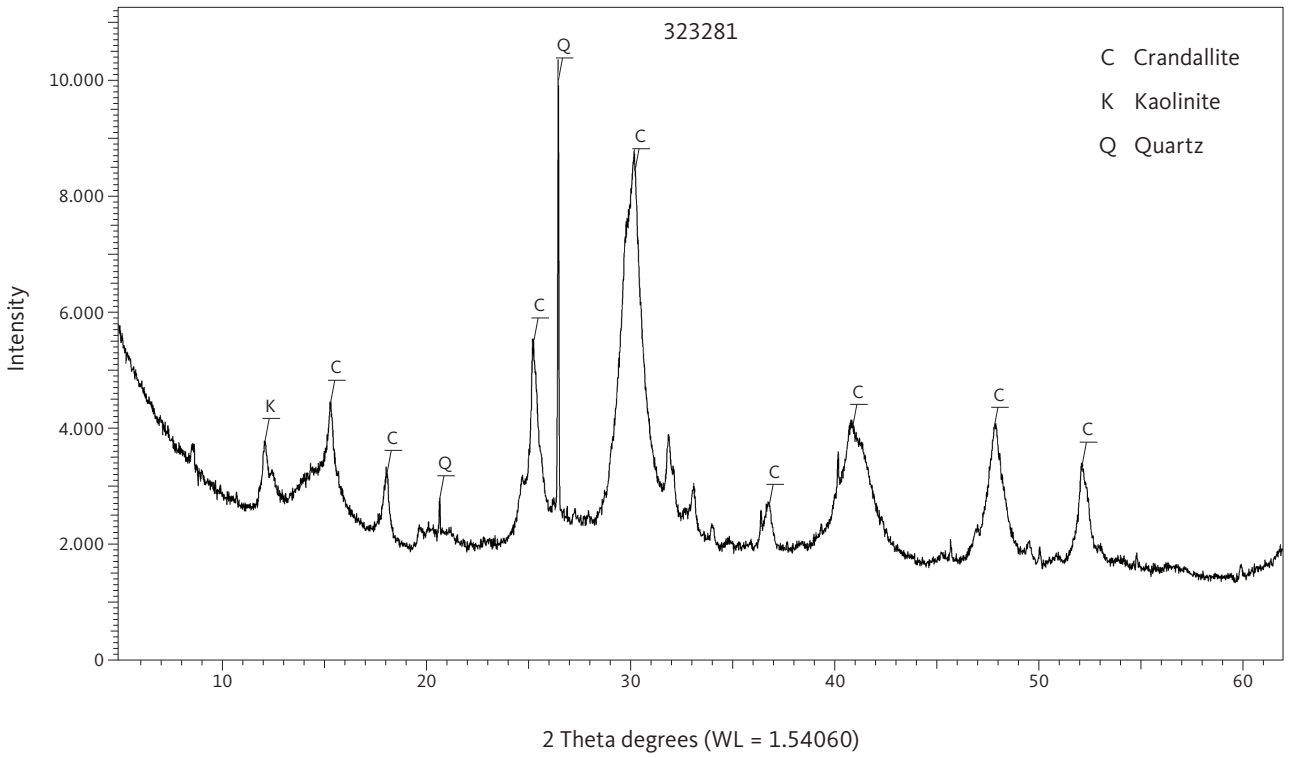

Fig. 11 X-ray diffractogram of sample 323281 from Nuugaarsuk, eastern Disko. The sample contains 18.26 wt% P_2O_5 (Table 2) and consists almost exclusively of crandallite, with small amounts of detrital quartz and kaolinite. A few small peaks are not identified.

5.5 Maximum alteration temperature

To estimate the temperature of the diagenetic processes involved in the crandallite formation, 40 random reflectance measurements of huminitic carbon particles were obtained for sample 323281, which is above the minimum of 20–30 measurements needed to get a reliable mean R_o value (Barker & Pawlewicz 1993). The mean R_o value of the sample is 0.43% (standard deviation 0.116). The R_o value is determined by the maximum heating temperature to which the organic matter has been subjected, which in most cases is controlled by increasing temperature associated with burial depth (e.g. Suggate 1998). Thermal maturation is an irreversible process, and the R_o values will thus always reflect the maximum temperature impact. In line with this, Barker & Pawlewicz (1994) established a relationship between R_o and peak burial temperature (T_{peak}). According to this relationship, the mean R_o of 0.43% corresponds to a maximum temperature of 68°C after deposition of the sample. This result is in excellent agreement with the 60–80°C for end-Eocene maximum temperatures obtained by thermochronology by Green *et al*. (2013, p. 79) for samples from the same area on Nuussuaq as investigated here.

6 Discussion

The environments in which crandallite forms are summarised by Dill (2001), who lists several different sedimentary environments ranging from superficial deposits in caves and bauxites over coal swamps to lacustrine deposits. Tuffs are commonly invoked, and there does seem to be a strong connection between tuff layers and phosphorus enrichment (cf. Section 1. Introduction). In all cases, percolating meteoric water is a necessary agent for the diagenetic processes, which lead to deposition of crandallite and its Sr-, Ba- and REE-analogues goyazite, gorceixite and florencite. Whereas there is agreement between various authors on the diagenetic origin of the crandallite group minerals, suggestions for the source of the elements, particularly phosphorus, range from volcanic rocks through neighbouring sediments to organic material, or a combination of these. In successions with several crandallite layers, a mechanism for the periodic enrichments should also be considered.

In the Disko–Nuussuaq occurrences, the geological environment was lacustrine, the volcanic origin of the original tuff layers is proven, and the source and basaltic composition of the original tuff is known. Given a realistic original composition of the tuff, a quantification of the element changes in the tuff layers is thus possible. Remaining questions relate to the source of the enriched elements and the conditions and processes during which the crandallite formed.

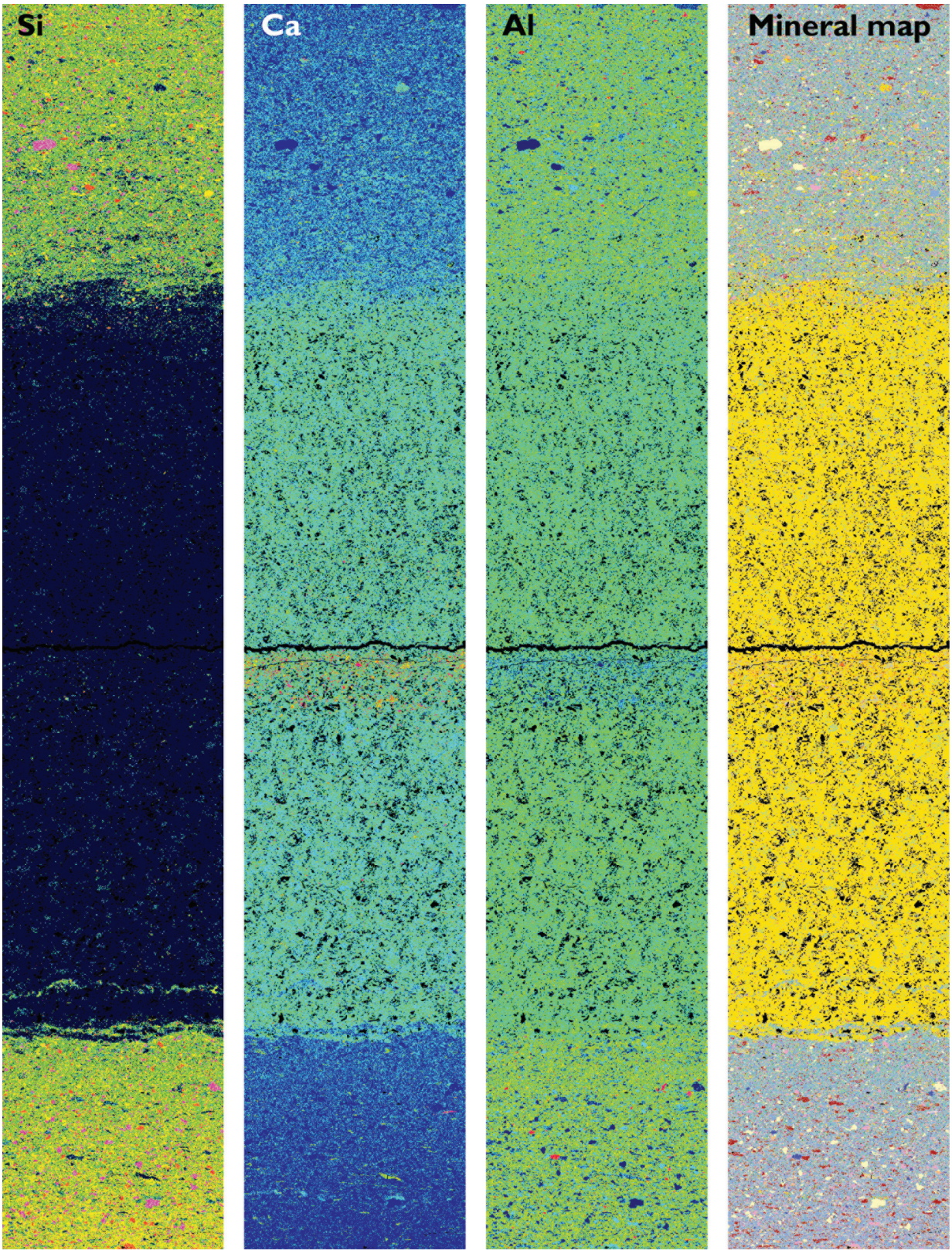

Fig. 12 SEM-AQM analysis traverse across tuff layer and lower and upper adjacent mudstones in thin section of sample 323267: Three element maps (Si, Ca, Al) and an AQM mineral map with legends in Fig. 13. Length of the traverse 20 mm; its position is shown in Fig. 6. The P map (not shown) is similar to the Ca map. The tuff layer itself comprises only the central part with extremely low Si content. The base is down, the top is up. Note the gradual increase in Si away from the tuff layer in both the lower and upper adjacent mudstones. The **red grains** in the Si map are quartz. The higher Ca and lower Al in the zone below the crack in the middle of the tuff are caused by an increased amount of apatite. The mineral map is strongly dominated by crandallite (**bright yellow**) in the tuff. Note that the upper mudstone contains crandallite in decreasing amounts away from the tuff, whereas the lower mudstone contains no or very little crandallite. The mudstones are dominated by kaolinite (**pale blue**). Quartz is **pale yellow**. Fe-oxide is **dark red**. The few **dark blue** grains in the lower mudstone were suggested by the AQM software to be mineral X, but the XRD analyses show that they are gibbsite; both minerals have Al as the only cation (**red** in the Al map) and cannot be distinguished by the SEM.

Table 1 Automated quantitative mineralogy of tuff layers and sidewalls, area%.

GGU-no	323256	323267	323281	349620	349621-1	349621-2
Profile	Akunneq 5	Akunneq 5	Nuugaarsuk	Eqip I.Qaqq	Eqip I.Qaqq	Eqip I.Qaqq
Member	Pingu Mb	Pingu Mb	Pingu Mb	Naujât Mb	Naujât Mb	Naujât Mb
Tuff layer					Lower section	Upper section
Crandallite	78.79	82.47	79.76	48.90	47.84	78.59
Crandallite(Fe)[a]	0.74	0.37	1.11	5.58	8.72	3.45
Gorceixite	2.37	3.39	4.15	1.03	0.65	0.99
Mix (AlSiCaPO)[b]	4.16	0.43	0.40	1.11	0.52	1.01
Apatite	0.01	0.85	2.24	0	0	0
Mineral X	0	0	0	38.14	31.92	5.34
Kaolinite	1.06	0	0	0.32	0.09	0.04
Quartz	0.24	0	1.93	0	0	0
'Holes'[c]	11.04	11.84	9.80	4.36	9.86	10.13
Sum[d]	98.41	99.35	99.39	99.44	99.6	99.55
Sidewall	**323256**	**323267**	**323281**	**349620**	**No sidewall in section**	
	Below tuff	Below tuff	Above tuff	Below tuff		
Kaolinite	21.74	29.17	12.6	31.78		
Mix (AlSiCaPO)[b]	40.57	23.72	40.62	22.76		
Mixes (AlSiO ± Ca)[e]	5.58	7.86	2.61	11.13		
Crandallite	9.37	1.62	14.26	1.33		
Crandallite(Fe)	1.17	0.85	8.67	0.52		
Gorceixite	0.5	0.13	1.27	0.03		
Mineral X	0	0	0	9.99		
Quartz	4.36	6.97	0.63	1.95		
Fe-oxides/hydroxides	3.63	6.22	5.71	5.72		
K-feldspar	1.72	2.8	0.41	1.43		
Ca-Na-feldspar	2.13	4.9	1.24	2.36		
Micas (bi + mus)	2.51	3.75	1.75	3.41		
Clays	2.52	6.25	3.44	3.99		
Gibbsite	1.33	1.86	0.69	0		
Chlorite	0.6	1.1	0.19	0.31		
Calcite	0.63	0.72	0.04	0.84		
Apatite	0.03	0.03	0	0		
'Holes'[c]	0.24	0.23	2.01	1.07		
Sum[d]	98.63	98.18	96.14	98.62		

[a]Crandallite with some Fe substituting for Ca or Al; [b]Unresolved fine-grained mixture of kaolinite/clays and crandallite; [c]Holes' comprise pore spaces and organic carbon; [d]Small amounts of ilmenite, baryte, siderite and tourmaline(?) are not included; [e]Unresolved fine-grained mixture of kaolinite/clays and plagioclase?

6.1 Quantification of element changes in tuff layers

A calculation of element changes in the tuff layers is shown in Table 3, based on analytical averages. We chose a basaltic composition as the best representative of the original composition of the tuff, because even in an erupting picrite the glass is of basaltic composition (Larsen & Pedersen 2000). Further, olivine and chromite crystals undergo aeolian fractionation during an eruption and tend to be deposited close to the eruption site. The rare chromites found in the thin sections support this, and the basalt average used in Table 3 has very nearly the same Cr content as the average altered tuff. A picritic original composition would have lower SiO_2, TiO_2 and Al_2O_3 and higher MgO and Cr; this would slightly change the magnitudes but not the directions of the change, and Cr would have been lost.

The most remarkable of the calculated element changes in Table 3 are the large losses of SiO_2 and the large gains of H_2O and P_2O_5. Around 65 wt% of the mass of the tuff layer has been replaced by other elements. The least mobile major elements were Al and Ca, which reacted with P to form crandallite. Al and Ca are almost the only major elements which originally resided in the volcanic deposits, and even some aluminium has been added to the tuff.

Of the trace elements, Cr reflects the source basalt and is apparently close to immobile during the alteration. The REE and multi-element diagrams show large differences between original and altered tuff layers (Fig. 15). Besides Cr, the only trace or minor elements in the tuffs, which could originally have resided in the volcanic rocks, are Nb, Ta, Zr, Hf and Ti. The mudstones could have been the source of Rb, Ba, Th, K, Pb, REE and also Zr, Hf and Ti.

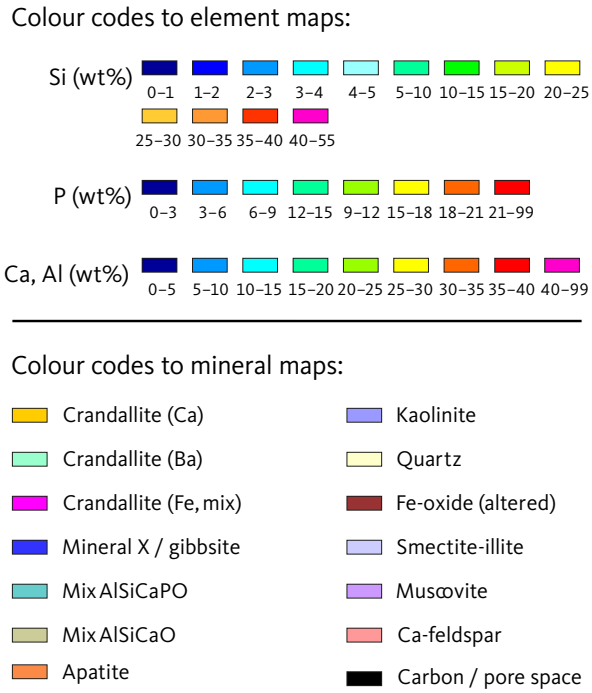

Fig. 13 Legend for the SEM-AQM analysis traverses in Figs 12 and 14. The mixed minerals are explained in Table 2.

6.2 Source of enriched elements

Of the enriched elements in Table 3, H_2O and Al do not present an explanatory problem because the processes took place at or below a lake bottom, and Al was present in sufficient quantities in both the volcanic material and the surrounding sediment. But the source of P, Ba, Sr, REE and C requires consideration. In addition, the tuff layers containing mineral X contain measurable quantities of nitrogen.

6.2.1 Phosphorus

Concentrations of P_2O_5 in crandallite-rich tuff layers up to 18.3 wt% (Table 2) necessitate external sources for the phosphorus. Phosphorus enrichment in coal swamp environments is widespread (Spears *et al*. 1988; Reinink-Smith 1990; Ward *et al*. 1996; Kokowska-Pawlowska & Nowak 2013; Dai *et al*. 2015). As the coals themselves are poor in phosphorus, most studies suggest that the phosphorus was derived from organic matter during peat decay, whereas some suggest an additional volcanic input (Spears *et al*. 1988; Ward *et al*. 1996; Reinhardt *et al*. 2013). On the other hand, Dai *et al.* (2015) explicitly state that in the occurrences they describe "no evidence of input from volcanic activity as a source of the phosphorus-bearing minerals has been observed".

Phosphorus-enriched layers in sedimentary successions without coals have been explained as follows: (1) transported grains of detrital origin from regolith (Wilson 1985); (2) sourced from dissolution of apatite (Bonnot-Courtois & Flicoteaux 1989; Pe-Piper & Dolansky 2005); (3) altered apatite from a carbonatitic tuff layer (Kiipli *et al*. 2012) and (4) biogenic, caused by environmental (climatic) disruptions due to explosive volcanic events (Mach *et al*. 2021).

The crandallite-rich tuff layers in the Libkovice Member, Czech Republic (Mach *et al*. 2021), and those in the Disko–Nuussuaq region have very similar settings in large, long-lived lakes. Significant differences between the two are that in Czechia the supposed eruption sites were situated more than 500 km away, and the magmas were silicic. Further, the Libkovice Member contains only three thick and a few thinner tuff layers, in contrast to the up to 20 tuff layers in the Disko–Nuussuaq succession. Mach *et al*. (2021) suggested that the crandallite beds were formed in long-lasting drought periods during which sediment transport to the lake was blocked, so that organic material could accumulate undiluted on the lake floor. These periods were triggered by volcanic eruptions in a warming climate in the beginning of the Miocene Climatic Optimum. This process may be conceivable for occurrences with a few crandallite layers, but for West Greenland we consider around 20 climatic oscillations due to only moderately explosive hydromagmatic activity to be unlikely.

The tuff layers in the Naajaat–Pingu lake formed through a number of short-lived volcanic eruptions, whereas the siliciclastic sedimentation was in principle continuous. Indeed, the top parts of several tuff layers comprise mixtures of volcanic and siliciclastic material, which was probably swept into the lake immediately after an eruption. For some layers, the crandallite formation extends a few millimetres into the overlying mudstone (e.g. Fig. 12), and to a lesser degree also into the underlying mudstone. Crandallite formation is in all previous studies considered to be an early diagenetic process, and we similarly envisage that the process took place soon after the tuff layer was deposited and covered with a veneer of new mudstone. The phosphorus-rich material probably became available in connection with the volcanic eruptions.

As noted in Section 5.4, the basement in the region east of the Naajaat–Pingu lake and also the volcanic areas west of the lake are very low in P and Sr (less so in Ba) and are not realistic candidates for the source of the periodic enrichments demonstrated in Table 3. No carbonatite volcanism at the time is known from the region. The only likely source for the enrichment is therefore organic material, as in the coal-bearing environments and in the Libkovice Member (Mach *et al*. 2021).

Marine plant plankton has empirical ratios of carbon:nitrogen:phosphorus of 106:16:1 (the Redfield ratio); the P content of marine plant plankton is thus less than 1 wt% dry weight (Redfield 1958). Land plants

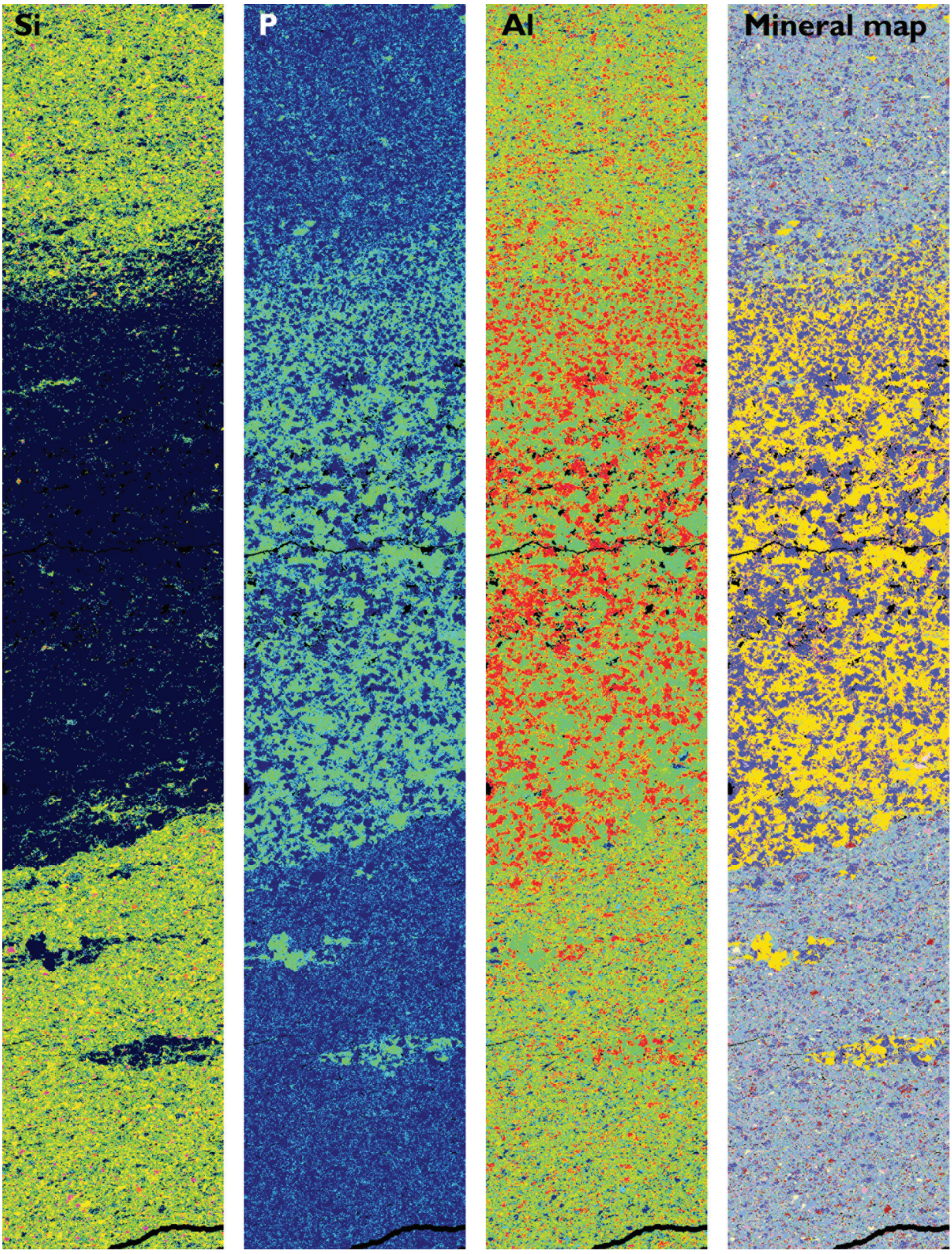

Fig. 14 SEM-AQM analysis traverse across tuff layer and lower and upper adjacent mudstones in thin section of sample 349620: three element maps (Si, P, Al) and an AQM mineral map with legends in Fig. 13. Length of the traverse *c*. 9 mm; its position is shown in Fig. 6. The Ca map (not shown) is similar to the P map. The tuff layer itself comprises only the central part with very low Si content. The base is down, the top is up. Two distinct patches in the lower mudstone are burrow-like. The Si map shows somewhat diffuse boundaries of the tuff and the occurrence of patches of silicate within the tuff. The Al map shows a mineral with extremely high Al (**bright red**: up to 40 wt% Al) and no Si, P or Ca; this is mineral X. The mineral map shows that the tuff layer consists of around equal amounts of intergrown crandallite (**bright yellow**) and mineral X (**dark blue**). The burrow-like patches below the tuff consist of crandallite and mineral X like the tuff itself. The adjacent mudstones are dominated by kaolinite (**pale blue**), which also forms the silicate patches within the tuff. Crandallite occurs in the upper mudstone but not in the lower mudstone except in the burrow-like patches. In contrast, mineral X occurs in minor amounts in both upper and lower mudstones.

Table 2 Chemical analyses of tuff layers and mudstones.

GGU-no	349598	349616	349620	349625	323236	323237	323263	323281	349593	323253	323289
Profile	Kingittoq4	Eqip I.Qaqq	Eqip I.Qaqq	Eqip I.Qaqq	Akunneq1	Akunneq1	Akunneq5	Nuugaarsuk	Kingittoq	Akunneq5	Akunneq7
Member	Naujât Mb	Naujât Mb	Naujât Mb	Naujât Mb	Pingu Mb	Pingu Mb	Pingu Mb	Pingu Mb	Naujât Mb	Pingu Mb	Assoq Mb
Rock	Tuff	Tuff	Tuff	Tuff	Tuff	Tuff	Tuff	Tuff	Mudstone	Mudstone	Mudstone
Major elements, XRF, wt%											
SiO_2	8.48	0.41	3.65	10.13	8.77	10.11	8.83	4.59	41.88	34.76	41.51
TiO_2	0.49	1.58	0.40	0.19	1.00	1.31	0.66	0.63	1.11	1.04	1.22
Al_2O_3	26.64	37.08	28.80	29.28	24.81	24.05	24.6	24.83	25.01	29.09	27.67
Fe_2O_3	0.87	12.75	0.88	0.16	2.62	1.40	0.96	2.37	8.28	11.56	7.11
MnO	0.04	0.003	0.004	0.007	0.12	0.03	0.03	0.14	0.10	0.24	0.16
MgO	0.65	0.09	0.35	0.46	0.58	0.73	0.67	0.57	0.85	0.73	1.08
CaO	9.76	1.15	4.54	9.70	8.72	7.89	8.58	11.11	0.66	0.76	0.88
Na_2O	0.04	0.02	0.05	0.04	0.14	0.24	0.17	0.24	0.35	0.23	0.48
K_2O	0.30	0.21	0.30	0.07	0.30	0.37	0.26	0.15	1.65	0.89	1.07
P_2O_5	16.93	2.23	7.35	15.23	15.17	13.85	14.63	18.26	0.14	0.26	0.17
Volatiles	32.65	44.05	47.55	32.20	33.42	35.12	36.48	31.83	19.39	20.89	18.88
Sum	96.85	99.58	93.86	97.47	95.65	95.10	95.87	94.72	99.42	100.45	100.23
TC	9.49	4.47	9.85	8.59	8.35	9.71	10.23	8.13	6.85	5.00	5.10
TS	0.08	2.55	0.06	0.12	0.02	0.04	0.11	0.08	n.a.	n.a.	n.a.
Trace elements, ICP-MS, ppm											
Sc	26.1	12.3	16.4	15.4	30.1	28.0	26.4	31.6	17.6	22.4	25.0
V	120	409	163	39.2	149	305	171	187	141	219	282
Cr	395	714	289	140	339	326	221	301	150	192	170
Co	9.95	6.56	10.6	7.27	29.9	17.9	31.6	18.1	28.0	35.7	31.9
Ni	25.0	90.2	35.5	22.2	41.6	23.6	75.6	25.6	78.9	84.3	71.1
Cu	74.6	458	346	23.8	108	125	273	108	55.6	67.7	84.1
Zn	70.4	63.1	404	136	73.9	98.1	100	81.6	108	97.4	125
Ga	43.2	50.7	45.9	44.2	42.1	47.8	39.8	42.7	35.4	38.3	37.3
Rb	11.1	0.99	17.1	1.51	11.0	14.0	11.1	5.83	66.0	36.5	41.1
Sr	3005	491	2830	2200	8155	10 668	7862	11 909	106	125	104
Y	240	37.4	106	250	136	100	109	107	22.5	26.2	21.0
Zr	47.7	24.8	57.2	20.8	52.6	78.9	54.1	50.7	225	84.1	124
Nb	5.31	24.3	7.42	3.38	16.2	19.6	7.52	7.72	18.0	13.0	14.6
Cs	0.434	0.055	0.733	0.114	0.458	0.578	0.416	0.257	2.42	1.80	1.63
Ba	18 594	2187	5705	12 601	15 571	18 569	17 510	19 806	556	395	437
La	182	121	228	120	68.9	137	165	75.9	53.7	61.6	60.9
Ce	551	296	529	274	198	336	370	202	108	131	129
Pr	70.5	37.6	60.9	40.5	29.9	41.0	42.1	24.9	11.5	12.5	13.9
Nd	346	151	251	227	143	178	178	112	41.0	43.8	49.7
Sm	73.1	21.0	45.9	83.4	31.0	37.8	33.3	22.7	7.16	7.69	8.51
Eu	17.8	4.41	13.0	21.4	7.67	8.48	8.33	4.73	1.61	1.74	1.89
Gd	73.7	15.9	53.7	81.4	31.6	33.1	31.6	22.6	5.76	6.46	6.86
Tb	9.30	1.84	5.92	9.35	4.10	4.06	4.10	3.09	0.822	0.937	0.954
Dy	48.1	8.55	25.3	50.2	23.0	20.7	21.4	17.2	4.25	4.92	4.77
Ho	8.30	1.30	4.02	8.90	4.27	3.43	3.88	3.25	0.796	0.929	0.877
Er	18.5	3.17	7.50	19.6	10.5	8.14	8.66	8.13	2.10	2.48	2.13
Tm	1.81	0.330	0.786	1.97	1.23	0.939	0.973	1.02	0.327	0.358	0.317
Yb	7.84	1.73	3.81	8.64	6.36	4.96	4.88	5.55	2.03	2.24	1.93
Lu	0.835	0.234	0.464	0.900	0.804	0.657	0.605	0.816	0.294	0.319	0.276
Hf	1.46	0.713	1.59	0.866	1.67	2.23	1.65	1.47	5.55	2.44	3.21
Ta	0.320	0.784	0.473	0.425	0.505	0.645	0.388	0.263	1.13	0.774	0.884
Pb	78.5	17.0	86.6	54.8	10.2	13.6	18.6	7.77	24.5	30.3	27.1
Th	18.0	7.78	15.0	39.3	10.1	9.59	12.5	5.47	11.7	13.4	13.6
U	11.5	9.28	8.58	4.44	20.0	18.9	15.5	21.0	4.76	3.05	4.83

Fe_2O_3: All iron as Fe_2O_3; TC: Total carbon; TS: Total sulfur; n.a.: not analysed.

contain 0.05–0.5 wt% dry weight P (Vance *et al*. 2003), and there is no reason that limnic plankton should contain more P. Fossil remains of land plants are frequent in the Naujât Member (e.g. Koch 1959), and much of the carbon in both mudstones and tuffs may have originated in land plants swept into the lake from its quite large catchment area, possibly in higher amounts than usual during hydromagmatic eruptions. The plant material represented in the mudstones and tuffs (Fig. 8C) may have contributed some additional P to the tuff, but its low P content is far from the amount necessary to explain our results. The P content is higher in

Table 3 Enrichment factors and losses and gains during diagenesis.

wt%	[a]Ordl. Mb basalt	[b]Tuff layer	[c]Tuff/ basalt	Tuff – basalt	wt%	[d]Tuff – basalt	Losses and gains
SiO_2	49.75	7.67	0.15	−42.08	*SiO_2*	*−42.08*	
TiO_2	2.10	0.71	0.34	−1.39	*FeOT*	*−10.13*	
Al_2O_3	14.45	25.70	1.78	11.25	*MgO*	*−6.67*	
FeO_{Total}	11.39	1.26	0.11	−10.13	*CaO*	*−2.63*	
MnO	0.18	0.06	0.33	−0.12	*Na_2O*	*−2.19*	
MgO	7.28	0.61	0.08	−6.67	*TiO_2*	*−1.39*	*wt% lost*
CaO	11.92	9.29	0.78	−2.63	*MnO*	*−0.12*	*−65.21*
Na_2O	2.34	0.15	0.06	−2.19	K_2O	0.00	Stable
K_2O	0.24	0.24	1.00	0.00	TC	9.09	
P_2O_5	0.21	15.68	74.67	15.47	Al_2O_3	11.25	
[e]TC	-	9.09	-	9.09	P_2O_5	15.47	
[f]H_2O	-	24.65	-	24.65	H_2O	24.65	
Sum	99.86	95.11	-	−4.75			
ppm					**wt%**		
Ba	37	17 108	462	17 071	BaO	1.91	
Sr	244	7300	30	7056	SrO	0.83	
Ce	21	322	15	301	Ce_2O_3	0.04	wt% gained
Y	36	157	4	121	Y_2O_3	0.02	63.25
Cr	277	287	1	10			
ppm	**[g]Mudstone**	**[b]Tuff layer**	**[c]Tuff/ mudstone**				
Ba	476	17 108	36				
Sr	105	7300	70				
Ce	104	322	3				
Y	25.5	157	6				

[a]Average of 8 Ordlingassoq Mb basalts with MgO < 9 wt%. TC and H_2O are negligible in degassed basalt; [b]Average of 6 tuff layers with SiO_2 < 10 wt%; [c]Enrichment factor; [d]Column arranged by increasing difference, except for the trace elements; italic text: losses, underlined text: gains, all other text: neutral; [e]Total carbon; [f]H_2O in tuff is calculated as loss on ignition – TC; [g]Average of 14 mudstones from the Naujât and Pingu Members.

zooplankton and fish tissues, up to 5.7 wt%, but Mach *et al*. (2021) showed that even when these two sources were included in the calculations, it was still not possible to concentrate the necessary P to form the crandallite beds in the Libkovice Member from a single event. Therefore, they concluded that each crandallite bed was formed over a considerable time interval with no siliciclastic sedimentation.

Bone material consists of hydroxyapatite and approximately 22 wt% collagen, and fish bones contain *c*. 18.5 wt% P (dry weight, Goldschmidt 1958, p. 460), that is, 42.4 wt% P_2O_5. If a volcanic eruption into the Naajaat–Pingu lake led to mass mortality in the lake, fish bones (also teeth and scales) could have accumulated on the lake floor along with the tuff. Immediately after a volcanic eruption, rain and streams would wash a mixture of siliciclastic and volcanic material into the lake from the surrounding land areas (see upper part of tuff layer 323281, Fig. 6). This material would rapidly cover tuff and bones, thereby sealing the layer off from the biological cycle in the lake. The decomposed soft tissues could also have been sealed off but may have had better chances of being recycled into the lake. Crandallite contains *c*. 34 wt% P_2O_5, so that a massive crandallite layer would require a bone layer of a similar thickness, or less. The bones would break down, as seen in experiments with bottom sediments and water in Lake Erie (Nriagu 1983), and the diagenetic formation of crandallite could start very soon after deposition.

At the time of publication and to the authors' knowledge, no remains of fossil fish have ever been recorded from the Naujât and Pingu Member mudstones, despite dedicated searches for teeth and bones by expert palaeontologists. All fish parts seem to have broken down. This is in contrast to the overlying Assoq Member mudstones, in which concretions with fish bones and scales have been found on Nuussuaq (Koch 1959, p. 14; unpublished data by AKP and LML), and shells of the brackish-water mussel *Nucula* sp. have been found in eastern Disko (Larsen & Pedersen 1988). The contrast suggests, perhaps not surprisingly, that an environment with efficient breakdown of bone material is a necessary prerequisite for formation of crandallite.

6.2.2 Strontium, barium and REE

Bone material contains significant amounts of Sr and could also be a source of the high Sr contents in the crandallite layers. However, bones could not have delivered the high Ba, REE and Y observed here. These elements may derive from the mudstone – as shown in Table 3 the enrichment factors tuff/mudstone for Ba and REE+Y are lower than the enrichment factors tuff/basalt for these

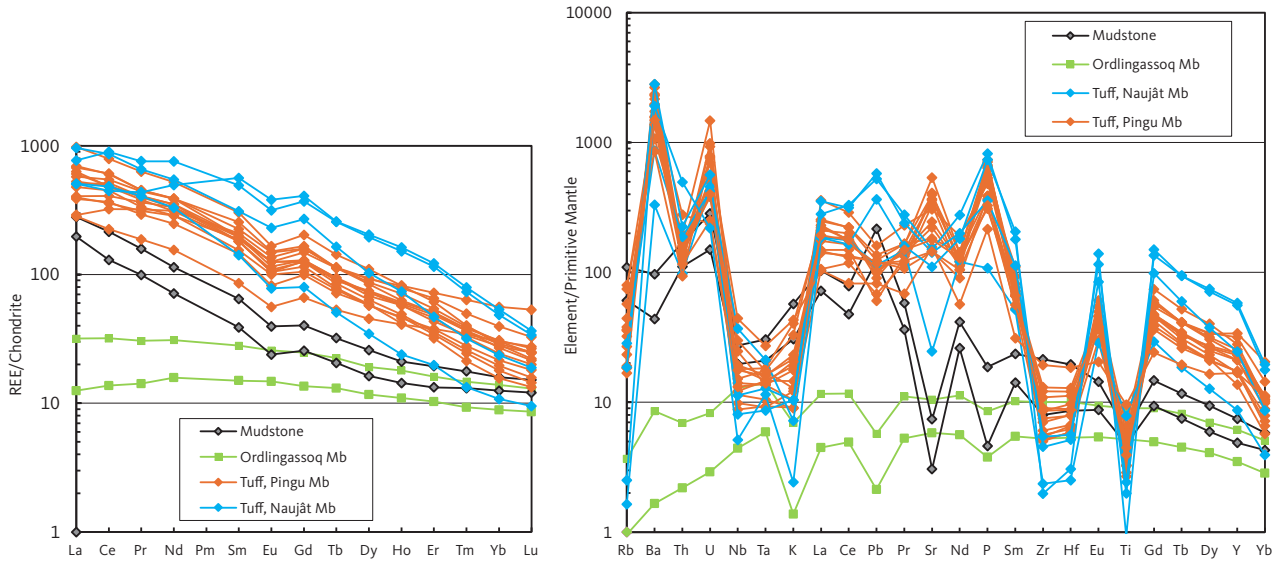

Fig. 15 REE- and multi-element diagrams for the tuffs compared with the surrounding mudstones and basaltic lavas of the Ordlingassoq Member of the Vaigat Formation. For mudstones and lavas, only the highest and lowest patterns are shown, defining the compositional intervals. Chondrite and Primitive Mantle normalisation factors from McDonough & Sun (1995). Mb: Member.

elements, for Ba by a factor of 10. A mudstone source is supported by the REE and multi-element patterns (Fig. 15), because the patterns for the tuff layers resemble those of the mudstones. In particular, both rock types have negative Eu anomalies, which contrasts with positive Eu anomalies in crandallite-altered tuff layers reported by von Gosen *et al.* (2019) and Mach *et al*. (2021). The similarly high Rb, Th, U and Pb in both tuff layers and mudstones likewise indicate that these elements originated in the mudstones. Indeed, a combined enrichment of Ba and REE by 100–1000% in bones decomposing by bone-soil-water interaction, with formation of crandallite, was observed by Trueman *et al*. (2004).

6.2.3 Carbon and nitrogen

The mudstones contain none or only very small amounts of carbonate (siderite, Table 1), and the tuff layers do not contain carbon-bearing minerals except for the few tuff layers containing mineral X. Thus, almost all carbon in both mudstones and tuff layers, up to 10 wt% (Table 2), must be in organic form and derived from biomass – plant material is indeed still identifiable (Fig. 8C). Carbon of course participated in the biological cycle in the lake and was continuously both added to and withdrawn from it, the withdrawal perhaps being higher in connection with the volcanic eruptions.

Mineral X contains roughly 10 wt% nitrogen identified by EDX analysis. A sample such as 349620, in which the tuff layer consists of about equal amounts of crandallite and mineral X, must contain around 5 wt% N. Nitrogen can only originate from biological material such as protein, and the approximately 22 wt% collagen in bone material contains approximately 16 wt% N (Huffman & Keil 2003), giving an amount of 4 wt% N in the total bone material. The fish bones we suggest have delivered the phosphorus and are thus an obvious candidate for delivery of the nitrogen too.

6.3 Diagenetic processes

As indicated by the low random reflectance of carbon particles in a tuff, the diagenetic processes in the sediments at the bottom of the lake took place at a low temperature, maximum 68°C. Considering the large amount of carbon in both tuff layers and mudstones (Table 2), the oxidation state during the diagenesis would have been low. However, crandallite has been interpreted to form in both oxidising (Weibel 1998; Rao & Walsh 1999) and reducing (Rasmussen 1996) environments as well as in acid (Dill 2001) and basic environments (this work). Natural changes in pH values may perhaps have taken place.

Soon after deposition and isolation of the tuff and bone layers, decomposition of the organic matter would start, probably aided by microbial activity (e.g. Rasmussen 1996; Rao & Walsh 1999; Collins *et al*. 2002), and P would be released into the pore water. At the same time, the volcanic glass would decompose to a hydrated gel (Fisher & Schmincke 1984), releasing Al, Ca and Sr to interact with pore-water P and form crandallite, replacing the glass. In the process, Si, Fe and Mg were lost from the system to the fluid (Table 3). The replacement took place without compaction of the tuff layer except

for one layer (sample 323256, Fig. 6), which may have been physically deformed by sliding or slumping during the replacement process.

The crystalline volcanic clasts were similarly almost completely replaced by crandallite, whereas Fe-Ti oxides were altered to Fe-oxides and -hydroxides and Ti-oxides, and only chromite remained from the original mineral assemblage. The near-complete diagenetic breakdown of well-crystallised igneous silicates, and removal of Si, requires distinctly basic conditions (Blatt 1982); the Si was likely incorporated into newly formed kaolinite in the surrounding mudstones. Amorphous Si, present in the volcanic glass, is much more soluble than quartz (Blatt 1982), which may explain why the clastic quartz grains in tuff layers were not dissolved (Fig. 6).

The formation of Mineral X within a single *c*. 70 m thick section at Eqip Innaarsuata Qaqqaa (Fig. 4) must be induced by some special, local conditions. We surmise that its formation may be related to the large, extensive picrite sill that underlies the Eqip Innaarsuata Qaqqaa mountain (see Section 3.4). The intrusion of the sill could have set up hydrothermal activity through local fractures, which moved the physico-chemical conditions such as pH and Eh into the presently unknown stability field of mineral X.

In the absence of phosphorus, the hydrated volcanic glass would have crystallised to smectite and other clay minerals (Fisher & Schmincke 1984), as seen in the tuff layers from the Assoq Lake of the Maligât Formation. This difference between the Naajaat–Pingu lakes and the younger Assoq Lake indicates either different diagenetic environments in the lakes or tuff deposition in the Assoq Lake without mass mortality of fauna.

7 Conclusions

Paleocene mudstones in the Nuussuaq Basin, West Greenland, contain about 20 tuff layers deposited in the Naajaat and Pingu lakes of the Atanikerluk Formation (*c*. 61 Ma). The tuffs were sourced from contemporaneous volcanoes of the Ordlingassoq Member of the Vaigat Formation, which erupted in part directly into the lake.

The tuffs were originally of basaltic to picritic composition but are thoroughly diagenetically altered to crandallite, $CaAl_3(PO_4)_2(OH)_5{\cdot}H_2O$, which in most tuffs comprises more than 80% of the rock and has replaced all original glass and igneous minerals except chromite. The tuffs contain up to 18 wt% P_2O_5 and have high contents of Sr (up to 24 600 ppm), Ba (up to 19 800 ppm) and REE (Ce up 550 ppm). These elements represent the Ba, Sr and REE analogues gorceixite, goyazite and florencite, which are in solid solution in the crandallite.

Using the compositions of an average Ordlingassoq Member basalt and an average mudstone-free tuff, chemical enrichment factors for tuff/basalt can be calculated. These are Ba: 462, P: 74.7, Sr: 30, Ce: 15, Al: 1.78. Further, on average, 9 wt% carbon and 24 wt% water have been added, and in total around 65 wt% of the mass of the tuff layer, mainly SiO_2, has been replaced by other elements. The least mobile major elements were Al and Ca, which reacted with P to form crandallite.

The source of phosphorus and carbon, as well as nitrogen, must be organic tissue in which these elements are major components. For such high concentrations as found in the tuffs, the determining element is P, and only bone material, including teeth and scales, contains sufficient P to form the crandallite-rich layers within a geologically short time. We suggest that the volcanic eruptions into the Naajaat–Pingu lake led to episodes of mass extinction in the lake, causing fish bones (also teeth and scales) to accumulate on the lake floor in association with the tuff. Clastic sediments would rapidly cover tuff and bones and seal the layer off from the biological cycle in the lake. Bone material could also be a source of the high Sr contents in the crandallite layers, whereas Ba, REE and Y would be derived from the surrounding mudstones.

The common association of tuff layers with crandallite in a hydrous environment is brought about by two conditions: an abundance of easily decomposed volcanic glass and an abundance of organic material rich in phosphorus such as bone. The abundance of both components may be caused by volcanic eruptions.

Additional information

Funding statement
All expenses in connection with this work were covered by the Geological Survey of Greenland (GGU) and its successor, the Geological Survey of Denmark and Greenland (GEUS).

Author contributions
LML, GKP, AKP: Conceptualisation, investigation (geology, petrography, rock chemistry), writing (lead), editing.
NK, SNM: Investigation (SEM analyses), writing, editing.
MBR: Investigation (XRD analyses), writing, editing.
HIP: Investigation (petrography, vitrinite reflectance), writing, editing.

Competing interests
The authors declare no competing interests.

Additional files
Four supplementary files are available at *https://doi.org/10.22008/FK2/TEA9HH*. These are: Supplementary file S1: Rock geochemical analyses, full set; Supplementary file S2: Figure: SEM-AQM analysis traverse of thin section, sample 323256; Supplementary file S3: Figure: SEM-AQM analysis traverse of thin section, sample 323281; Supplementary file S4: Figure: SEM-AQM analysis traverse of thin section, sample 349621.

Acknowledgements

The samples in this study were collected during geological investigations and mapping by AKP, LML and GKP in the 1980s, organised by the Geological Survey of Greenland (GGU; now the Geological Survey of Denmark and Greenland, GEUS). The samples were so unusual that they were put aside for further studies at a later time. The authors

are much indebted to Jørgen Bojesen-Koefoed (GEUS), Henrik Friis (Oslo) and Rikke Weibel (GEUS), all of whom we thank for their discussions and contributions of invaluable expert knowledge in their fields. Reviewers Lutz Reinhardt and Vladislav Rapprich are thanked for their constructive comments and suggestions, which led to improvement of the manuscript.

References

Barker, C.E. & Pawlewicz, M.J. 1993: An empirical determination of the minimum number of measurements needed to estimate the mean random vitrinite reflectance of disseminated organic matter. Organic Geochemistry **20**, 643–651. *https://doi.org/10.1016/0146-6380(93)90050-L*

Barker, C.E. & Pawlewicz, M.J. 1994: Calculation of vitrinite reflectance from thermal histories and peak temperatures. A comparison of methods. In: Mukhopadhyay, P.K. & Dow, W.G. (eds): Vitrinite reflectance as a maturity parameter. Applications and limitations. ACS Symposium Series **570**, 216–229. *https://pubs.acs.org/doi/abs/10.1021/bk-1994-0570.ch014#*

Blatt, H. 1982: Sedimentary petrology. New York: W.H. Freeman & Co.

Bonnot-Courtois, C. & Flicoteaux, R. 1989: Distribution of rare-earth and some trace elements in Tertiary phosphorites from the Senegal Basin and their weathering product. Chemical Geology **75**, 311–328. *https://doi.org/10.1016/0009-2541(89)90004-1*

Bøggild, O.B. 1918: Den vulkanske Aske i Moleret samt en Oversigt over Danmarks ældre Tertiærbjærgarter. Danmarks Geologiske Undersøgelse, II Række, vol. **33**, 159 pp. *https://doi.org/10.34194/raekke2.v33.6818*

Collins, M.J. *et al*. 2002: The survival of organic matter in bone: A review. Archaeometry **44**(3), 383–394. *https://doi.org/10.1111/1475-4754.t01-1-00071*

Dai, S., Hower, J.C., Ward, C.R., Guo, W., Song, H., O'Keefe, J.M.K., Xie, P. Hood, M.H. & Yuan, X. 2015: Elements and phosphorus minerals in the middle Jurassic inertinite-rich coals of the Muli Coalfield on the Tibetan Plateau. International Journal of Coal Geology **144–145**, 23–47. *https://doi.org/10.1016/j.coal.2015.04.002*

Dam, G. & Sønderholm, M. 2021: Tectonostratigraphic evolution, palaeogeography and main petroleum plays of the Nuussuaq Basin: An outcrop analogue for the Cretaceous–Palaeogene rift basins offshore West Greenland. Marine and Petroleum Geology **129**, 33 pp. *https://doi.org/10.1016/j.marpetgeo.2021.105047*

Dam, G., Pedersen, G.K., Sønderholm, M.S., Midtgaard, H.H., Larsen, L.M., Nøhr-Hansen, H. & Pedersen, A.K. 2009: Lithostratigraphy of the Cretaceous–Paleocene Nuussuaq Group, Nuussuaq Basin, West Greenland. Geological Survey of Denmark and Greenland Bulletin **19**, 1–171. *https://doi.org/10.34194/geusb.v19.4886*

Dam, G., Sønderholm, M. & Sørensen, E.V. 2020: Inherited basement canyons: Impact on sediment distribution in the North Atlantic. Terra Nova **32**(4), 272–280. *https://doi.org/10.1111/ter.12459*

Dill, H.G. 2001: The geology of aluminium phosphates and sulphates of the alunite group minerals: A review. Earth-Science Reviews **53**, 35–93. *https://doi.org/10.1016/S0012-8252(00)00035-0*

Fisher, R.V. & Schmincke, H.-U. 1984: Pyroclastic rocks. 472 pp. Berlin: Springer Verlag. *https://doi.org/10.1007/978-3-642-74864-6*

Flicoteau, R. & Lucas, J. 1984: Weathering of phosphate minerals. In: Nriagu, J.O. & Moore, P.B. (eds): Phosphate minerals. 292–317. Berlin, Heidelberg: Springer. *https://doi.org/10.1007/978-3-642-61736-2_9*

Goldschmidt, V.M. 1958: Geochemistry. 730 pp. London: Oxford University Press.

Green, P.F., Lidmar-Bergström, K., Japsen, P., Bonow, J.M. & Chalmers, J.A. 2013: Stratigraphic landscape analysis, thermochronology and the episodic development of elevated, passive continental margins. Geological Survey of Denmark and Greenland Bulletin **30**, 1–150. *https://doi.org/10.34194/geusb.v30.4673*

Gregersen, U., Knutz, P.C., Nøhr-Hansen, H., Sheldon, E. & Hopper, J.R. 2019: Tectonostratigraphy and evolution of the West Greenland continental margin. Bulletin of the Geological Society of Denmark **67**, 1–21. *https://doi.org/10.37570/bgsd-2019-67-01*

Gregersen, U. *et al.* 2022: Stratigraphy of the West Greenland margin. In: Dafoe, L.T. & Bingham-Koslowski, N. (eds): Geological synthesis of Baffin Island (Nunavut) and the Labrador–Baffin Seaway. Geological Survey of Canada Bulletin **608**, 247–309. *https://doi.org/10.4095/321849*

Haggerty, S.E. 1976: Opaque mineral oxides in terrestrial igneous rocks. Chapter 8 (pp Hg-101 to Hg-175) In: Rumble, D. (ed.): Oxide minerals. Berlin, Boston: De Gruyter. *https://doi.org/10.1515/9781501508561-013*

Huffman, E.W.D. & Keil, R.L. 2003: Determination of trace organic carbon and nitrogen in the presence of carbonates in anorganic bovine bone graft materials. Microchemical Journal **74**, 249–256. *https://doi.org/10.1016/s0026-265x(03)00031-6*

ICCP (International Committee for Coal and Organic Petrology) 2001: The new inertinite classification system (ICCP System 1994). Fuel **80**, 459–471. *https://doi.org/10.1016/S0016-2361(00)00102-2*

Keulen, N, Malkki, S.N. & Graham, S. 2020: Automated quantitative mineralogy applied to metamorphic rocks. Minerals **10**, 47, 29 pp. *https://doi.org/10.3390/min10010047*

Kiipli, T., Radzievicius, S., Kallaste, T., Kiipli, E., Siir, S., Soesoo, A. & Voolma, M. 2012: The Geniai Tuff in the southern East Baltic area – A new correlation tool near the Aeronian/Telychian stage boundary, Llandovery, Silurian. Bulletin of Geosciences **87**(3), 10 pp. *https://doi.org/10.3140/bull.geosci.1313*

Koch, B.E. 1959: Contribution to the stratigraphy of the non-marine Tertiary deposits on the south coast of the Nûgssuaq Peninsula, northwest Greenland, with remarks on the fossil flora. Bulletin Grønlands Geologiske Undersøgelse **22**, 100 pp. *https://doi.org/10.34194/bullggu.v22.6555*

Kokowska-Pawlowska, M. & Nowak, J. 2013: Phosphorus minerals in tonstein; coal seam 405 at Sośnica-Makoszowy coal mine, Upper Silesia, southern Poland. Acta Geologica Polonica **63**, 271–281. *https://doi.org/10.2478/agp-2013-0012*

Kystol, J. & Larsen, L.M. 1999: Analytical procedures in the Rock Geochemical Laboratory of the Geological Survey of Denmark and Greenland. Geology of Greenland Survey Bulletin **184**, 59–62. *https://doi.org/10.34194/ggub.v184.5230*

Larsen, L.M. & Pedersen, A.K. 1988: Investigations of Tertiary volcanic rocks along the south coast of Nûgssuaq and in eastern Disko, 1987. Rapport Grønlands Geologiske Undersøgelse **140**, 28–32. *https://doi.org/10.34194/rapggu.v140.8028*

Larsen, L.M. & Pedersen, A.K. 1992: Volcanic marker horizons in the upper part of the Maligât Formation on eastern Disko and Nuussuaq, Tertiary of West Greenland: Syn- to post-volcanic basin movements. Rapport Grønlands Geologiske Undersøgelse **155**, 85–93. *https://doi.org/10.34194/rapggu.v155.8186*

Larsen, L.M. & Pedersen, A.K. 2000: Processes in high-Mg, high-T magmas: Evidence from olivine, chromite and glass in Paleogene picrites from West Greenland. Journal of Petrology **41**, 1071–1098. *https://doi.org/10.1093/petrology/41.7.1071*

Larsen, L.M., Pedersen, A.K. & Pedersen, G.K. 2006: A subaqueous rootless cone field at Niuluut, Disko, Paleocene of West Greenland. Lithos **92**, 20–32. *https://doi.org/10.1016/j.lithos.2006.03.043*

Mach, K., Rapprich, V., Faměra, M., Havelcová, M., Grygar, T.M., Novotný, T., Řehoř, M. & Kochergina, Y.V.E. 2021: Crandallite-rich beds of the Libkovice Member, Most Basin, Czech Republic: Climatic extremes or paleogeographic changes at the onset of the Miocene Climatic Optimum? Geologica Acta **19**, 1–29, I–X. *https://doi.org/10.1344/GeologicaActa2021.19.11*

McDonough, W.F. & Sun, S.-S. 1995: The composition of the Earth. Chemical Geology **120**, 223–253. *https://doi.org/10.1016/0009-2541(94)00140-4*

Nøhr-Hansen, H. 2025: The Cretaceous to Eocene: A biostratigraphical review and a new detailed palynostratigraphy of Greenland and adjacent areas. Palynology **49**(1), 80 pp. *https://doi.org/10.1080/01916122.2024.2377158*

Nriagu, J.O. 1983: Rapid decomposition of fish bones in Lake Erie sediments. Hydrobiologica **106**, 217–222. *https://doi.org/10.1007/bf00008119*

Ottley, C.J., Pearson, D.G. & Irvine, G.J. 2003: A routine method for the dissolution of geological samples for the analysis of REE and trace elements via ICP-MS. In: Holland, J.G. & Tanner, S.D. (eds): Plasma source mass spectrometry: Applications and emerging technologies. 221–230. Cambridge: Royal Society of Chemistry. *https://doi.org/10.1039/9781847551689-00221*

Pedersen, A.K., Larsen, L.M. & Dueholm, K.S. 1993: Geological section along the south coast of Nuussuaq, central West Greenland. 1:20 000 coloured geological sheet. Copenhagen: Geological Survey of Greenland. *https://doi.org/10.22008/FK2/AUDF7K*

Pedersen, A.K., Larsen, L.M., Pedersen, G.K. & Dueholm, K.S. 1996: Filling and plugging of a marine basin by volcanic rocks: The Tunoqqu Member of the Lower Tertiary Vaigat Formation on Nuussuaq, central West Greenland. Bulletin Grønlands Geologiske Undersøgelse **171**, 5–28. *https://doi.org/10.34194/bullggu.v171.6731*

Pedersen, A.K., Larsen, L.M. & Dueholm, K.S. 2002: Geological section along the north side of the Aaffarsuaq valley and central Nuussuaq, central West Greenland. 1:20 000 coloured geological sheet. Copenhagen: Geological Survey of Denmark and Greenland. *https://doi.org/10.22008/FK2/FJJ3MG*

Pedersen, A.K., Larsen, L.M., Pedersen, G.K. & Dueholm, K.S. 2005: Geological section across north central Disko from Nordfjord to Pingu, central West Greenland. 1:20 000 coloured geological sheet. Copenhagen: Geological Survey of Denmark and Greenland. *https://doi.org/10.22008/FK2/SDHFT3*

Pedersen, A.K., Larsen, L.M., Pedersen, G.K., Sønderholm, M., Midtgaard, H.H., Pulvertaft, T.C.R. & Dueholm, K.S. 2006: Geological section along the north coast of the Nuussuaq peninsula, central West Greenland. 1:20 000 coloured geological sheet. Copenhagen: Geological Survey of Denmark and Greenland. *https://doi.org/10.22008/FK2/ZY5WBS*

Pedersen, A.K., Pedersen, G.K., Larsen, L.M., Pulvertaft, T.C.R., Sønderholm, M. & Dueholm, K.S. 2007a: Geological map of the Nuussuaq Basin in southern Nuussuaq, 1:100 000, special map Paatuut, with detailed sections. Copenhagen: Geological Survey of Denmark and Greenland. *https://doi.org/10.22008/FK2/KE1GCB*

Pedersen, A.K., Pedersen, G.K., Larsen, L.M., Pulvertaft, T.C.R., Sønderholm, M. & Dueholm, K.S. 2007b: Geological map of the south-east coast of Nuussuaq between Ataata Kuua and Saqqaqdalen, central West Greenland, 1:50 000, with detailed sections. Copenhagen: Geological Survey of Denmark and Greenland. *https://doi.org/10.22008/FK2/V9AHQN*

Pedersen, A.K., Larsen, L.M. & Pedersen, G.K. 2017: Lithostratigraphy, geology and geochemistry of the volcanic rocks of the Vaigat Formation on Disko and Nuussuaq, Paleocene of West Greenland. Geological Survey of Denmark and Greenland Bulletin **39**, 1–244. *https://doi.org/10.34194/geusb.v39.4354*

Pedersen, A.K., Larsen, L.M. & Pedersen, G.K. 2018: Lithostratigraphy, geology and geochemistry of the volcanic rocks of the Maligât Formation and associated intrusions on Disko and Nuussuaq, Paleocene of West Greenland. Geological Survey of Denmark and Greenland Bulletin **40**, 1–239. *https://doi.org/10.34194/geusb.v40.4326*

Pedersen, G.K., Larsen, L.M., Pedersen, A.K. & Hjortkjær, B.F. 1998: The synvolcanic Naajaat lake, Paleocene of West Greenland. Palaeogeography, Palaeoclimatology, Palaeoecology **140**, 271–287. *https://doi.org/10.1016/s0031-0182(98)00034-0*

Pe-Piper, G. & Dolansky, L.M. 2005: Early diagenetic origin of Al phosphate-sulfate minerals (woodhouseite and crandallite series) in terrestrial sandstones, Nova Scotia, Canada. American Mineralogist **90**, 1434–1441. *https://doi.org/10.2138/am.2005.1790*

Rao, P.D. & Walsh, D.E. 1999: Influence of environments of coal deposition on phosphorus accumulation in a high latitude, northern Alaska, coal seam. International Journal of Coal Geology **38**, 261–284. *https://doi.org/10.1016/s0166-5162(98)00026-3*

Rasmussen, B.R. 1996: Early-diagenetic REE-phosphate minerals (florencite, gorceixite, crandallite and xenotime) in marine sandstones: A major sink for oceanic phosphorus. American Journal of Science **296**, 601–632. *https://doi.org/10.2475/ajs.296.6.601*

Redfield, A.C. 1958: The biological control of chemical factors in the environment. American Scientist **46**(3), 205–221. *https://www.jstor.org/stable/27827150*

Reinhardt, L., Estrada, S., Andruleit, H., Dohrmann, R., Piepjohn, K., von Gosen, W., Davis, D.W. & Davis, B. 2013: Altered volcanic ashes in Palaeocene and Eocene sediments of the Eureka Sound Group (Ellesmere Island, Nunavut, Arctic Canada). Zeitschrift der Deutschen Gesellschaft für Geowissenschaften **164**(1), 131–147. *https://doi.org/10.1127/1860-1804/2013/0004*

Reinink-Smith, L.M. 1990: Mineral assemblages of volcanic and detrital partings in Tertiary coal beds, Kenai peninsula, Alaska. Clays and Clay Minerals **38**(1), 97–108. *https://doi.org/10.1346/CCMN.1990.0380113*

Spears, D.A., Duff, P.M.L.D. & Caine, P.M. 1988: The West Waterberg tonstein, South Africa. International Journal of Coal Geology **9**, 221–233. *https://doi.org/10.1016/0166-5162(88)90014-6*

Storey, M., Duncan, R.A., Pedersen, A.K., Larsen, L.M. & Larsen, H.C. 1998: $^{40}Ar/^{39}Ar$ geochronology of the West Greenland Tertiary volcanic province. Earth and Planetary Science Letters **160**, 569–586. *https://doi.org/10.1016/s0012-821x(98)00112-5*

Suggate, R.P. 1998: Relations between depth of burial, vitrinite reflectance and geothermal gradient. Journal of Petroleum Geology **21**, 5–32. *https://doi.org/10.1111/j.1747-5457.1998.tb00644.x*

Trueman, C.N.G., Behrensmeyer, A.K., Tuross, N. & Weiner, S. 2004: Mineralogical and compositional changes in bones exposed on soil surfaces in Amboseli National Park, Kenya: Diagenetic mechanisms and the role of sediment pore fluids. Journal of Archaeological Science **31**, 721–739. *https://doi.org/10.1016/j.jas.2003.11.003*

Vance, C.P., Uhde-Stone, C. & Allan, D.L. 2003: Phosphorus acquisition and use: Critical adaptations by plants for securing a nonrenewable resource. New Phytologist **157**, 423–447. *https:// doi.org/10.1046/j.1469-8137.2003.00695.x*

von Gosen, W., Reinhardt, L., Piepjohn, K. & Schmitz, M.D. 2019: Paleogene sedimentation and Eurekan deformation in the Stenkul Fiord area of southeastern Ellesmere Island (Canadian Arctic): Evidence for a polyphase history. In: Piepjohn, K. *et al.* (eds): Circum-Arctic Structural Events: Tectonic Evolution of the Arctic Margins and Trans-Arctic Links with Adjacent Orogens. Geological Society of America Special Paper **541**, 325–348. *https://doi.org/10.1130/2018.2541(16)*

Ward, C.R., Corcoran, J.F., Saxby, J.D. & Read, H.W. 1996: Occurrence of phosphorus minerals in Australian coal seams. International Journal of Coal Geology **30**, 185–210. *https://doi.org/10.1016/0166-5162(95)00055-0*

Weibel, R. 1998: Diagenesis in oxidising and locally reducing conditions – An example from the Triassic Skagerrak Formation, Denmark. Sedimentary Geology **121**, 259–276. *https://doi.org/10.1016/s0037-0738(98)00085-2*

Wilson, J.A. 1985: Crandallite group minerals in the Hekilian Athabasca Group in Alberta, Canada. Canadian Journal of Earth Science **22**, 637–641. *https://doi.org/10.1139/e85-065*